**Title: An essential periplasmic protein coordinates lipid trafficking and is required for asymmetric polar growth in mycobacteria**

**Authors:** Kuldeepkumar R. Gupta[a], Celena M. Gwin[a], Kathryn C. Rahlwes[b], Kyle J. Biegas[d,e], Chunyan Wang[a,c], Jin Ho Park[a], Jun Liu[a,c], Benjamin M. Swarts[d,e], Yasu S. Morita[b], and E. Hesper Rego[a,1]

**Affiliations**

[a] Department of Microbial Pathogenesis, Yale University School of Medicine, New Haven, CT 06519

[b] Department of Microbiology, University of Massachusetts, Amherst, MA 01003

[c] Microbial Sciences Institute, Yale University, West Haven, CT 06516

[d] Department of Chemistry and Biochemistry, Central Michigan University, Mount Pleasant, MI 48859

[e] Biochemistry, Cell, and Molecular Biology Program, Central Michigan University, Mount Pleasant, MI 48859

[1]To whom correspondence should be addressed: hesper.rego@yale.edu

**ABSTRACT**

Mycobacteria, including the human pathogen *Mycobacterium tuberculosis*, grow by inserting new cell wall material at their poles. This process and that of division are asymmetric, producing a phenotypically heterogeneous population of cells that respond non-uniformly to stress (Aldridge et al., 2012; Rego et al., 2017; Richardson et al., 2016). Surprisingly, deletion of a single gene – *lamA* – leads to more symmetry, and to a population of cells that is more uniformly killed by antibiotics (Rego et al., 2017). How does LamA create asymmetry? Here, using a combination of quantitative time-lapse imaging, bacterial genetics, and lipid profiling, we find that LamA recruits essential proteins involved in cell wall synthesis to one side of the cell – the old pole. One of these proteins, MSMEG_0317, here renamed PgfA, was of unknown function. We show that PgfA is a periplasmic protein that interacts with MmpL3, an essential transporter that flips mycolic acids in the form of trehalose monomycolate (TMM), across the plasma membrane. PgfA interacts with a TMM analog suggesting a direct role in TMM transport. Yet our data point to a broader function as well, as cells with altered PgfA levels have differences in the abundance of other lipids and are differentially reliant on those lipids for survival. Overexpression of PgfA, but not MmpL3, restores growth at the old poles in cells missing *lamA*. Together, our results suggest that PgfA is a key regulator of polar growth and cell envelope composition in mycobacteria, and that the LamA-mediated recruitment of this protein to one side of the cell is a required step in the establishment of cellular asymmetry.

45 **INTRODUCTION**

46 *Mycobacterium tuberculosis* (Mtb), the etiological agent of human tuberculosis
47 (TB), is responsible for approximately 1.4 million deaths each year. One of the pathogen's
48 distinguishing features is its unusual cell envelope. Like nearly all other bacterial species,
49 the plasma membrane is surrounded by peptidoglycan, a rigid mesh-like structure made
50 up of carbohydrate chains crosslinked by peptide bridges. However, in contrast to the
51 peptidoglycan of other well-characterized bacteria, mycobacterial peptidoglycan is
52 covalently linked to the highly branched hetero-polysaccharide arabinogalactan, which is,
53 itself, covalently bound to extremely long-chained fatty acids called mycolic acids.
54 Collectively, this structure is known as the mycolyl-arababinogalactan-peptidoglycan
55 complex or mAGP. Electron microscopy has revealed that the outer most layer is a lipid
56 bilayer, and, as such, it is referred to as the outer membrane, or, alternatively, the
57 mycomembrane (Hoffmann et al., 2008; Zuber et al., 2008). In addition to this core
58 structure, several lipids, lipoglycans, and glycolipids, are abundantly and non-covalently
59 interspersed across the plasma membrane and mycomembrane (Jackson, 2014; Jankute
60 et al., 2015). This complex cell envelope is a double-edged sword: it is a formidable barrier
61 to many antibiotics yet provides several potentially targetable structures. Indeed, two of
62 the four first-line TB antibiotics target cell envelope biosynthesis.

63 In addition to their unusual cell envelope, mycobacteria differ from other well-
64 studied rod-shaped bacteria in important ways. Notably, mycobacteria elongate by adding
65 new material at their poles rather than along their side walls. Over the course of a cell
66 cycle, one pole grows more than the other, giving rise to an asymmetric growth pattern
67 (Aldridge et al., 2012). Importantly, closely related organisms like corynebacteria that

68 have similar cell wall architecture grow more evenly from their poles, suggesting that
69 asymmetry is not simply a consequence of polar growth and may be actively created by
70 mycobacteria (Rego et al., 2017). In fact, while the molecular details of asymmetric polar
71 growth are not yet well understood (Baranowski et al., 2019; Kieser and Rubin, 2014), we
72 have discovered that LamA, a protein of unknown function specific to the mycobacterial
73 genus, is involved (Rego et al., 2017). Deletion of *lamA* results in more growth from the
74 pole formed from the previous round of division, “the new pole”, and less from the
75 established growth pole, “the old pole”, leading to less asymmetry (Fig. 1A) (Rego et al.,
76 2017).

77 To understand LamA’s role in mycobacterial division and elongation, we identified
78 multiple putative LamA-interacting proteins of known and unknown function (Rego et al.,
79 2017). One of these proteins, MSMEG_0317, is predicted to be associated with several
80 other divisome proteins (Wu et al., 2018) (Fig. 1A). Attempts to delete *msmeg_0317* from
81 the *Mycobacterium smegmatis* chromosome have been unsuccessful (Cashmore et al.,
82 2017), and transposon insertion mapping has predicted the *M. tuberculosis* homolog,
83 *rv0227c*, to be essential (DeJesus, M. A. et al., 2017; Zhang et al., 2012). MSMEG_0317
84 belongs to the DUF3068-domain super-family of proteins, which are exclusively found in
85 actinobacteria. One member of this family in corynebacteria has channel activity, so this
86 domain has been renamed PorA (Abdali et al., 2018; Soltan Mohammadi et al., 2013). In
87 addition, by structure-based homology prediction, MSMEG_0317 shares limited
88 homology to CD36, which transports long-chained fatty acids into eukaryotic cells (Patel
89 et al., 2022). In corynebacteria, the putative homolog of MSMEG_0317, LmcA, is thought

90 to have lipid binding activity (Patel et al., 2022), and is involved in an ill-defined step of
91 lipoglycan synthesis (Cashmore et al., 2017; Patel et al., 2022).

92 Here, we sought to understand the role of MSMEG_0317 in relation to LamA
93 during mycobacterial growth and division. We find that in *M. smegmatis*, a model
94 mycobacterial species, MSMEG_0317 is essential for polar growth, and localizes to the
95 old pole in a LamA-dependent manner. There, it localizes with MmpL3, the essential
96 mycolic acid flippase, to build the mycomembrane. Our data suggest that one function of
97 MSMEG_0317 is to traffic mycolic acids in the periplasmic space, and that its
98 overexpression is sufficient to restore growth at the old pole in cells missing *lamA*. With
99 only 21% sequence identity to MSMEG_0317, the putative corynebacterial homolog
100 LmcA cannot substitute for MSMEG_0317, suggesting that these proteins are not
101 orthologs, and that the function of MSMEG_0317 is specific to mycobacteria. Together,
102 these results implicate MSMEG_0317 in mycolic acid trafficking, and argue that it is an
103 important regulator of cell wall composition and incorporation at one site of growth – the
104 old pole – in mycobacteria. As such, we propose to rename MSMEG_0317, PgfA, for
105 Polar growth factor A.
106

107 **RESULTS**

108 **PgfA is essential for polar growth and localizes to the sites of new cell wall**
109 **synthesis**

110 To verify the essentiality of *pgfA* in *M. smegmatis*, we used an allele swapping
111 strategy (Pashley and Parish, 2003). Briefly, in a strain whose only copy of *pgfA* was at
112 the L5 phage integration site (Lewis and Hatfull, 2000; van Kessel and Hatfull, 2007), we

113 exchanged *pgfA* for either an empty vector or for another copy of itself (Fig. 1B).
114 Consistent with *pgfA* being essential for cell growth, we observed approximately 1000-
115 fold fewer colonies when we exchanged *pgfA* with an empty vector compared to
116 exchanging it for another copy of itself (Fig. 1B).

117 To visualize the morphology of *pgfA*-depleted cells, we constructed a strain in
118 which the only copy of the gene was tetracycline inducible (Fig. 1C; Figure 1 – figure
119 supplement 1A). Removal of anhydrotetracycline (ATC) from the culture media prevented
120 cell growth (Figure 1 – figure supplement 1A). By time-lapse microscopy we observed
121 that, while cells expressing PgfA became longer, on average, as cell density increased
122 within the microfluidic device (Fig. 1C; Figure 1 – figure supplement 1B) cells depleted for
123 PgfA stopped elongating but continued to divide (reductive division), became wider, and,
124 in many instances, eventually lysed (Fig. 1C, Figure 1 – figure supplement 1B).

125 To determine where and when PgfA functions in the cell, we fused PgfA to mRFP
126 and expressed the resulting chimera from the native *pgfA* promoter. By allele swapping,
127 we find that $P_{native}$-*pgfA-mrfp* restores bacterial growth (Figure 1 – figure supplement 1C)
128 and thus encodes a functional PgfA. Fluorescence microscopy at a single time-point
129 showed that PgfA-mRFP localizes to mid-cell and to the poles (Fig. 1D, Figure 1 – figure
130 supplement 2A). In polar growing bacteria, the site of division eventually becomes the site
131 of elongation. Thus, in addition to localizing to the poles, elongation-complex proteins can
132 also appear at mid-cell before daughter cell separation is clearly observed. This makes it
133 difficult to determine true septal-associated localization from a single time point. To
134 disentangle whether PgfA, in addition to localizing to the poles, also localizes to the

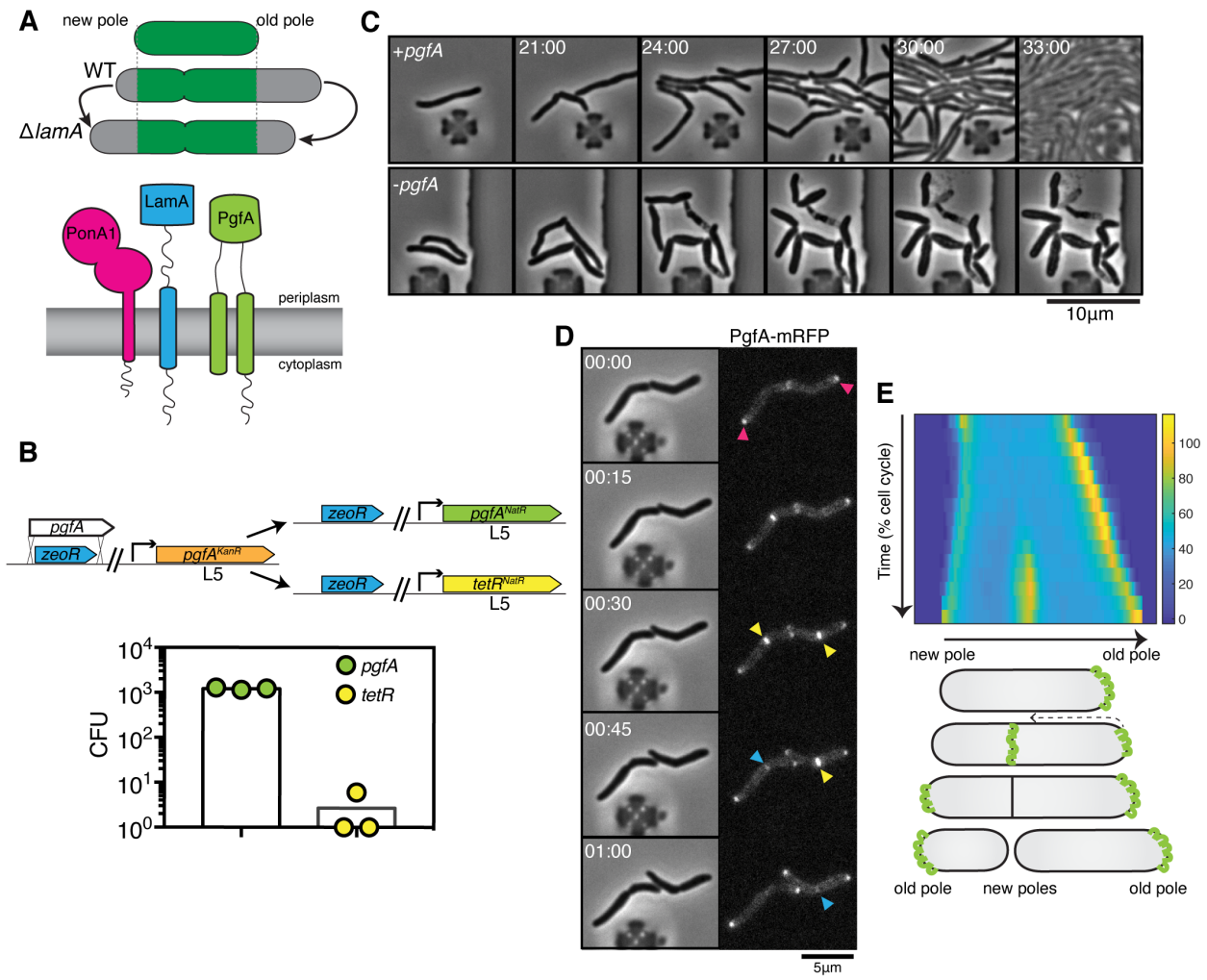


**Figure 1. PgfA is an essential polar growth factor that localizes asymmetrically. (A)** *top:* Graphical depiction of growth pattern in WT and Δ*lamA* cells. Green=old cell wall material. Grey= new cell wall material. *bottom*: LamA is a membrane protein that co-immuno-precipitates with PonA1, a bifunctional penicillin binding protein, and MSMEG_0317/PgfA, a protein of unknown function. **(B)** Schematic and results of allelic exchange experiment. Vectors with *pgfA* or without *pgfA* (*tetR*) were transformed into a strain whose only copy of *pgfA* was at the L5 integration site. Transformants carrying the incoming vectors were counted by colony forming units (CFU). **(C)** A strain whose only copy of PgfA is tetracycline-inducible was imaged over time with (+pgfA) or without (-pgfA) anhydrotetracycline (ATC). Cells were loaded into a microfluidic device 18 hours after the removal of ATC (bottom) or a mock control (top). **(D)** Cells whose only copy of PgfA was fused to mRFP, were imaged over time by phase and fluorescence microscopy in a microfluidic device with constant perfusion of media. **(E)** *Top*. Individual cells (N=25) were followed from birth to division and the fluorescence was measured from new to old pole. Each resulting kymograph was interpolated over cell length and time and then averaged together. Using this analysis, we find that PgfA is first at the old poles (pink triangles), partially re-localizes to the septum (yellow triangles) during cell division, and then disappears from the site of division before the next cell cycle (blue triangles) to establish asymmetry in the next generation. *Bottom*. A depiction of this localization pattern is shown as a cartoon.

septum during division, we visualized PgfA-mRFP by time-lapse microscopy (Fig. 1D). For a single cell, we measured the fluorescence distribution over time as a function of

137 both cell cycle time and cell length. As we wanted to compare across strains, we averaged
138 many of these individual trajectories together. The resulting 'average' kymograph
139 represents the probability of finding a fluorescent protein in a particular cellular location
140 at a particular stage of the cell cycle (Fig. 1E). Using this analysis, we compared the
141 spatiotemporal localization of PgfA-mRFP to the earliest known markers for the division
142 complex (FtsZ-mCherry2B) and the elongation complex (eGFP-Wag31) (Figure 1 – figure
143 supplement 2B). We find that PgfA localizes primarily to the old pole before the onset of
144 division. During division, the fluorescence intensity at the old pole becomes slightly less
145 intense as PgfA-mRFP re-localizes to the septum (Fig. 1D, E). This event occurs during
146 the latter stages of FtsZ recruitment, but before the arrival of Wag31 to the mid-cell,
147 suggesting that PgfA is a late divisome-associated protein (Figure 1 – figure supplement
148 2). At the end of division, PgfA-mRFP disappears from the septal site such that the new
149 daughter cells are once again born with an asymmetric distribution of PgfA (Fig. 1D, E).
150 Taken together, these data are consistent with PgfA being a member of both the
151 mycobacterial division and elongation complexes and show that PgfA is essential for polar
152 growth.
153

154 **PgfA and MmpL3 are recruited to the old pole by LamA to build the mycomembrane**

155 The manner of cell death suggested a defect in the cell envelope of PgfA-depleted
156 cells. To resolve the layers of the mycobacterial cell envelope in detail we used cryo-
157 electron microscopy (cryo-EM) to visualize frozen-hydrated cells. As has been previously
158 observed (Hoffmann et al., 2008; Zuber et al., 2008), wild type *M. smegmatis* cells exhibit

159 distinct plasma and outer membranes, both clearly observed as bilayers, separated by
160 approximately 50-nm (Fig. 2A). In cells depleted of PgfA, the outer membrane is frayed
161 (Fig. 2A and Figure 2 – figure supplement 1) and largely devoid of electron density (Fig.
162 2A). Thus, PgfA is important for maintaining the structural organization of
163 mycomembrane.

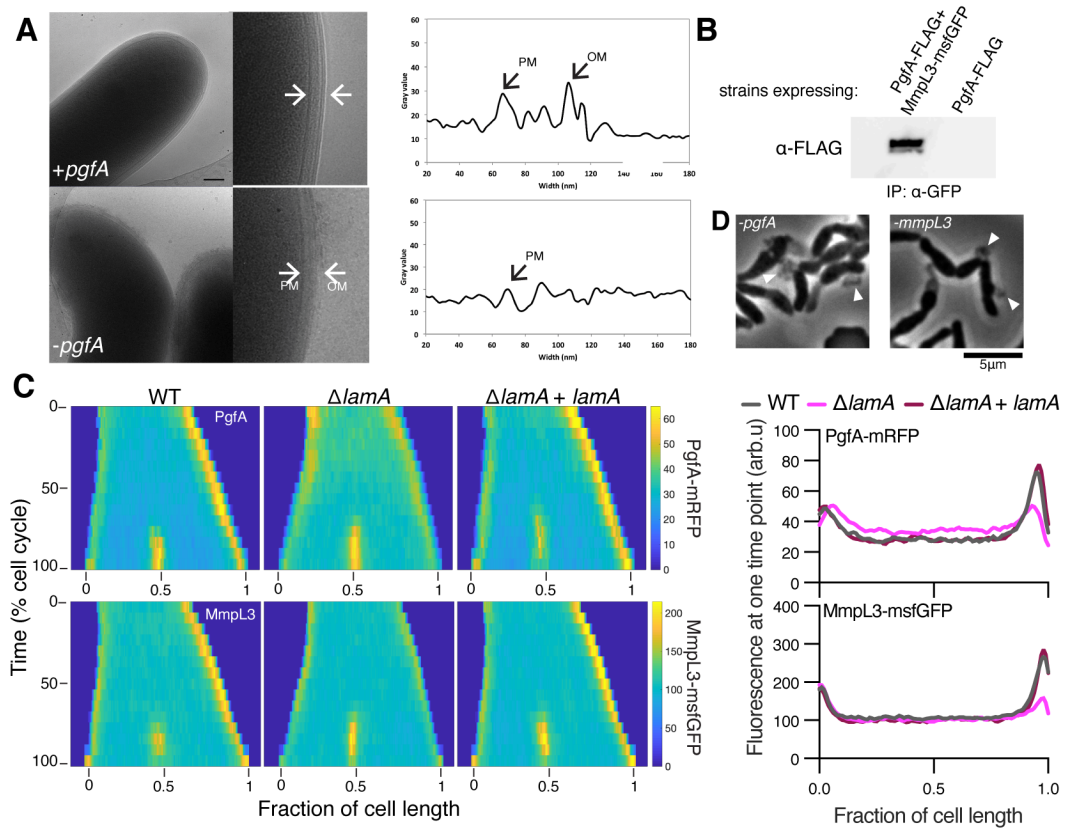


**Figure 2. LamA recruits PgfA and MmpL3 to the old pole to build the mycomembrane.** **(A)** The cell envelope of a representative wild type Msm cell and a cell depleted of PgfA for 24 hours were visualized and measured by cryo-electron microscopy. PM = plasma membrane; OM = outer membrane. Scale bar = 100 nm. **(B)** The lysates from strains expressing PgfA-FLAG with or without MmpL3-msfGFP were immuno-precipitated (IP) using GFP-trap beads, and the elution was probed for the presence of PgfA-FLAG via anti-FLAG Western blot. **(C)** *left*: Fluorescent protein fusions to either PgfA or MmpL3 were imaged by time-lapse microscopy in wildtype, Δ*lamA,* and complement cells (Δ*lamA* +pNative-*lamA*) N=25. The resulting images were then processed as described in Figure 1D. *right:* The same data as on the left is plotted at a single time point to show the decrease in old pole accumulation of MmpL3 and PgfA in the absence of *lamA.* **(D)** Cells were depleted using CRISPRi for *pgfA* or *mmpL3* and a representative timepoint is shown. Cell wall material is excreted from the poles and septa during depletion (white triangles).

164 Many of the cytoplasmic and periplasmic enzymes involved in mycomembrane
165 synthesis have been identified. However, the molecular details of how precursors are
166 trafficked from the plasma membrane to build the complex structure are almost
167 completely unknown. We do know that one key step involves the essential protein
168 MmpL3, which transports trehalose monomycolate (TMM) across the plasma membrane
169 to the periplasm (Su, C. C. et al., 2021; Xu et al., 2017). There, TMM is trafficked, through
170 unknown mechanisms, to the antigen 85 enzymes (Backus et al., 2014), and incorporated
171 onto mAGP or made into trehalose dimycolate (TDM), a component of the outer
172 mycomembrane leaflet (Chiaradia et al., 2017). Importantly, MmpL3 has become an anti-
173 TB therapeutic target, as multiple compounds have been found to inhibit its function
174 (Adams et al., 2021; La Rosa et al., 2012; Umare et al., 2021).

175 Using an *E. coli* two-hybrid approach, MmpL3 from *M. tuberculosis* was recently
176 found to interact with several factors involved in cell wall synthesis, growth, and division,
177 including Rv0227c (64% identity to *M. smegmatis* PgfA) (Belardinelli et al., 2019). To
178 verify that PgfA and MmpL3 interact in intact mycobacterial cells, we constructed strains
179 that expressed fusions to these proteins to enable co-immunoprecipitation. Precipitating
180 MmpL3-GFP with a nanobody against GFP, we found PgfA-FLAG in the elution only when
181 MmpL3-GFP was present (Fig. 2B). Taken together, these results show that MmpL3 and
182 PgfA interact in the cell.

183 As our initial interest in PgfA was prompted by its connection to LamA, we
184 wondered if PgfA and MmpL3 would localize differently in Δ*lamA* cells. Thus, we
185 visualized fluorescent fusions to PgfA and MmpL3 in strains with and without *lamA* and
186 analyzed the fluorescence distributions over time. MmpL3-msfGFP displayed the same

187 spatial and temporal localization pattern as PgfA-mRFP, again suggesting they are part
188 of the same complex (Fig. 2C). Surprisingly, in Δ*lamA* cells, PgfA-mRFP and MmpL3-
189 msfGFP became dramatically less abundant at the old pole, with no change in abundance
190 at the new pole. The loss of polar PgfA and MmpL3 in Δ*lamA* could be complemented by
191 integrating *lamA* at a single site on the chromosome (Fig. 2C). The abundance of
192 msfGFP-MurJ, which transports peptidoglycan precursors, was not as dramatically
193 changed at the old pole in Δ*lamA* cells, showing that the LamA-dependent loss of MmpL3
194 and PgfA was specific and not a general loss of elongation-complex proteins (Figure 2 –
195 figure supplement 2).

196 If PgfA and MmpL3 are functioning together, then cells depleted of either essential
197 protein may have the same terminal phenotype. To assay this, we created CRISPRi -
198 guides to both *mmpL3* and *pgfA* and visualized the morphology of cells over time as the
199 depletion was induced (Rock et al., 2017). As *pgfA* is predicted to be the first gene in a
200 two gene operon (Martini et al., 2019), we were concerned about polar effects of the
201 CRISPRi depletion (Rock et al., 2017). To address this, we integrated another copy of
202 MSMEG_0315, the second gene in the operon, at a phage site expressed by its native
203 promoter. Consistent with the notion that PgfA and MmpL3 function in the same pathway,
204 we found that cells depleted for *mmpL3* phenocopied those depleted for *pgfA* in that they
205 become progressively shorter and wider (Figure 2 - video supplement 1). By phase
206 contrast microscopy, we also observed cell wall material excreted from the poles and the
207 septa in both *mmpL3*- and *pgfA*- depleted cells (Fig. 2D). These observations are
208 reminiscent of cells treated with ethambutol (Wuo et al., 2022), a drug that inhibits the
209 synthesis of arabinan, the anchor point for mycolic acids, leading to accumulation and

210 shedding of TMM (Kilburn and Takayama, 1981; Mikusova et al., 1995). Indeed, inhibition
211 or depletion of MmpL3 leads to TMM accumulation (Degiacomi et al., 2017; Fay et al.,
212 2019a; Su, Chih-Chia et al., 2019; Tahlan et al., 2012).

213 Collectively, our data are consistent with a model in which LamA recruits PgfA and
214 MmpL3 to the old pole, either directly or indirectly, where they function to construct the
215 mycomembrane. Further, our data suggest that cells depleted for PgfA accumulate TMM,
216 possibly to toxic levels.

217

218 **PgfA is a periplasmic protein that binds TMM**

219 As our data suggested that PgfA-depleted cells accumulated TMM, we wondered
220 if PgfA was directly or indirectly interacting with TMM. A recent proteomics study identified
221 PgfA as a putative TMM-interacting protein (Kavunja et al., 2020). To verify this, we tested
222 whether PgfA could be captured from live *M. smegmatis* cells using N-x-AlkTMM-C15, a
223 synthetic photo-cross-linkable TMM analogue containing an alkyne "click" chemistry
224 handle that enables specific detection and/or enrichment of cross-linked protein
225 interactors (Kavunja et al., 2020). *M. smegmatis* cells expressing PgfA-3xFLAG were
226 incubated with N-x-AlkTMM-C15 and exposed to UV irradiation to effect cross-linking.
227 Then, cell lysates were collected and subjected to "click" reaction to dual label N-x-
228 AlkTMM-C15-modified proteins with fluorophore and biotin affinity tags. Biotinylated
229 proteins were captured on avidin beads, eluted, and analyzed by anti-FLAG Western blot.
230 We found that PgfA was enriched exclusively in N-x-AlkTMM-C15-treated, UV-exposed
231 *M. smegmatis*, demonstrating direct interaction between PgfA and the TMM analogue
232 (Fig. 3A and Figure 3 – figure supplement 1)

Several accessory proteins work with MmpL3 and/or are required to transport TMM across the plasma membrane. However, to date, all the known accessory proteins reside in the cytoplasm or have globular domains on the cytoplasmic side of the plasma membrane(Fay et al., 2019b). The topology of the predicted PgfA structure, shows a beta barrel-like domain anchored by one or, possibly two, transmembrane helices(Patel et al., 2022). Prediction of the orientation with respect to the membrane is ambiguous (Figure 3 – figure supplement 2A). To map the topology of PgfA, we fused mGFPmut3 to either the N- or the C-terminal side of PgfA (Fig. 3B). As GFP does not fluoresce in the mycobacterial periplasm,[36] we reasoned that fluorescence would indicate cytoplasmic localization of GFP. Importantly, both fusion

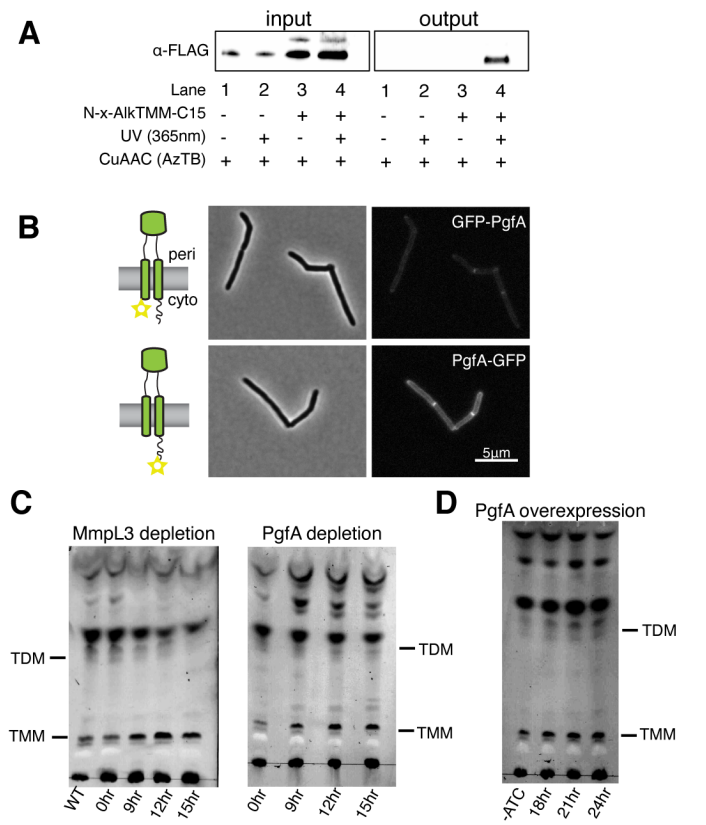


**Figure 3. PgfA is a periplasmic protein that binds TMM and is involved in TMM trafficking. (A)** Cells expressing PgfA-3xFLAG were cultured with N-x-AlkTMM-C15 (100 μM), UV-irradiated, and lysed. Lysates were reacted with azido-TAMRA-biotin reagent (AzTB) by Cu-catalyzed azide-alkyne cycloaddition (CuAAC "click" reaction), and analyzed before (input) and after (output) avidin bead enrichment by anti-FLAG Western blot. The full analysis, including Coomassie and in gel-fluorescence scanning is displayed in Figure 3 – figure supplement 1. Data are representative of two independent experiments. **(B)** PgfA is fused to GFPmut3 at either its N- or C- terminus and integrated into Msm as the sole copy of PgfA. Cells carrying these fusions are imaged by fluorescence microscopy. Images are displayed on identical intensity scales to allow direct comparison. **(C)** Using CRISPRi, cells were depleted of MmpL3 or PgfA at the indicated timepoints and the cell envelopes were analyzed for TMM and TDM by TLC. **(D)** Cells were induced to overexpress PgfA at the indicated timepoints, and their cell envelopes were analyzed by TLC for TMM and TDM. Data in C and D are representative from at two least independent experiments, all with similar results.

256 proteins can replace wild type PgfA at high efficiency, and thus encode functional PgfA
257 (Figure 3 – figure supplement 2B). Using fluorescence microscopy, we find that both the
258 N- and C-terminal fusions fluoresce, although the N-terminal fusion is significantly dimmer
259 (Fig. 3B). Nevertheless, collectively, these data show that PgfA is an inner membrane
260 protein with a large periplasmic domain and that it binds TMM.
261
262 **PgfA abundance correlates to altered TMM/TDM ratios**
263 If PgfA is involved in the trafficking of TMM, then its depletion, as with depletion of
264 MmpL3, should result in an altered TMM/TDM ratio (Degiacomi et al., 2017; Fay et al.,
265 2019; Su et al., 2019; Tahlan et al., 2012). Total cell-associated amounts of TMM and
266 TDM can be visualized by thin layer chromatography (TLC). As expected, depletion of
267 *mmpL3* leads to accumulation of TMM and a co-incident reduction of TDM (Fig. 3C). To
268 test if this is also the case for PgfA, we repeated the same procedure on cells depleted
269 of *pgfA*. In this case, we find that TMM accumulates while TDM levels are more stable
270 (Fig. 3C). These data are consistent with a model in which TMM accumulates in a different
271 subcellular compartment in *pgfA*-depleted cells, compared to *mmpL3*-depleted cells.
272 Specifically, it suggests that in *pgfA*-depleted cells, at least some of the TMM pool may
273 still be accessible to antigen 85 enzymes.
274 To further test the notion that PgfA is involved in TMM trafficking in the periplasm,
275 we created a strain which inducibly overexpressed the protein from a multi-copy plasmid.
276 Again, consistent with the notion that PgfA is involved in trafficking TMM, we find that
277 inducing the overexpression of PgfA results in increased TDM levels (Fig. 3D). Together

278 these data support a model in which PgfA functions as part of the TMM transport pathway
279 in the periplasm.
280
281 **The function of PgfA is specific to mycobacteria and its abundance negatively**
282 **correlates with the abundance of lipoglycans LM/LAM**
283 Our data indicate a role for PgfA in the transport of TMM. In contrast, the putative
284 corynebacterial homolog of *pgfA* has been proposed to function in the biosynthesis of two
285 large lipoglycans abundant in the mycobacterial cell envelope, lipomannan and
286 lipoarabinomannan (LM/LAM) (Cashmore et al., 2017). A deletion mutant of *NCgl2760*,
287 the presumed ortholog of *pgfA* in *C. glutamicum,* resulted in disappearance of LAM and
288 accumulation of truncated LM, which was clearly detectable by faster migration on SDS-
289 PAGE (Cashmore et al., 2017). To test if this is also the case in mycobacteria, we used
290 the same electrophoretic approach to analyze LM/LAM, and thin layer chromatography
291 (TLC) to examine potential changes in other lipid species upon depletion of *pgfA*. In
292 contrast to the results obtained in *C. glutamicum*, we observe a dramatic and transient
293 increase in the total amount of cell-associated LAM during depletion, before cells began
294 dying (Fig. 4A, Figure 4 – figure supplement 1). There were no obvious changes in the
295 migration of LM/LAM on SDS-PAGE, implying that the impact of PgfA depletion on
296 LM/LAM biosynthesis was minimal. Additionally, other lipids, including the precursor of
297 LM/LAM biosynthesis such as $AcPIM_2$, show no reproducible change (Figs. 4B,C; Figure
298 4 – figure supplement 1).

299 These data led us to hypothesize that PgfA and NCgl2760 are not orthologs,

300 despite the fact that there is synteny in their chromosomal location. However, while the

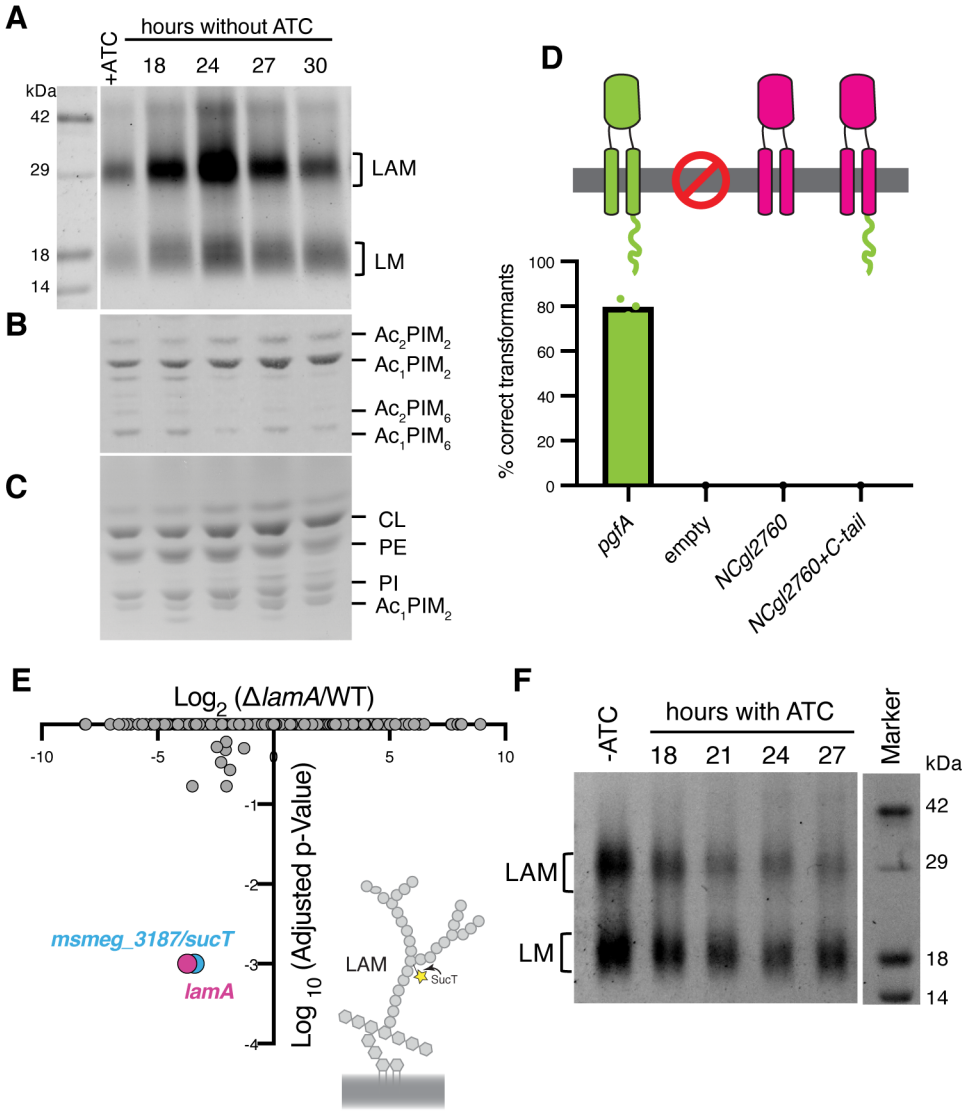


**Figure 4. LM/LAM levels negatively correlate with abundance of PgfA.** In a strain whose only copy of *pgfA* is ATC-inducible, **(A)** LM/LAM, **(B)** non-polar and polar PIMs, **(C)** and plasma membrane lipids were analyzed by **(A)** SDS-PAGE and **(B-C)** TLC during PgfA depletion (without ATC). Cell pellets were normalized by wet weight to account for differences in cell density. To avoid changes in LM/LAM due to cell density, at the indicated timepoints, half of the cultures were taken for lipid analysis, and replaced with fresh media. Two other biological replicates are shown in Figure 4 – figure supplement 1. CL, cardiolipin; PE, phosphatidylethanolamine; PI, phosphatidylinositol. **(D)** Results of exchanging the indicated *pgfA* and *C.glutamicum NCgl2760* alleles for a wildtype copy of *pgfA*. Correct transformants are positive for the incoming selective marker and negative for the outgoing (KanR, NatS). **(E)** Transposon insertions in Δ*lamA* comparted to WT. The only two genes with significantly different number of insertions (reduced) were *lamA* itself and *sucT*, a gene that codes for a protein known to modify LAM and arabinogalactan. **(F)** In cells carrying an ATC-inducible copy of *pgfA* on a multicopy plasmid, cell-associated LM/LAM were extracted, separated via SDS-PAGE, and visualized by ProQ Emerald with and without ATC at the indicated timepoints.

301 genes surrounding *NCgl2760* and *pgfA* share moderate to high degrees of sequence
302 identity (~30-50%), *NCgl2760* and *pgfA* are the clear outliers, with only 21% sequence
303 identity. In fact, a recent study solved the structure of the periplasmic domain of
304 MSMEG_0317 (PgfA) and compared it to the predicted AlphaFold (Jumper et al., 2021;
305 Varadi et al., 2022) structure of NCgl2760 and found differences in the size and shape of
306 the beta-barrel pocket (Patel et al., 2022). Additionally, NCgl2760 is missing the long C-
307 terminal cytoplasmic tail that is present in PgfA. Thus, we wondered if NCgl2760 can
308 substitute for PgfA in *M. smegmatis*. To test this, we first asked if PgfA's cytoplasmic tail
309 is important for its function using our allele swapping strategy (Fig. 1B). We find that
310 transformation of an allele deleted for this tail is inefficient (Figure 4 – figure supplement
311 2A), and that the few transformants that do survive have altered morphology (Figure 4 –
312 figure supplement 2B). Thus, the long C-terminal tail of PgfA is necessary for its function.
313 We next tried to swap alleles of NCgl2760 with or without the C-terminal PgfA tail.
314 Transformation of both genes was inefficient (Figure 4 – figure supplement 2C) and none
315 of the surviving transformants had correctly swapped out the parental *pgfA* gene (Fig.
316 4D). Thus, *NCgl2760*, even when coupled to the important cytoplasmic tail of PgfA,
317 cannot substitute for *pgfA* in *M. smegmatis*. These data indicate that PgfA and NCgl2760
318 may not be orthologs and could have diverged through evolution to perform different
319 functions.

320 Why does depletion of PgfA result in an accumulation of LM/LAM? To investigate
321 this, we decided to leverage Δ*lamA* cells, which naturally have less PgfA and MmpL3
322 (Fig. 2C). PgfA and MmpL3 have been described as highly vulnerable drug targets, *i.e.* a
323 small change in their abundance causes growth arrest or cell death (Bosch et al., 2021).

How do Δ*lamA* cells grow at a normal rate with fewer of these essential proteins? We reasoned that changes in gene essentiality in Δ*lamA* may uncover compensatory mechanisms that promote survival. Thus, we created transposon libraries in Δ*lamA* and wild type cells and compared insertions across the genomes. There were very few changes: aside from Δ*lamA* itself, the only gene that sustained significantly fewer insertions in Δ*lamA* across replicates was MSMEG_3187 or *sucT* (Fig. 4E, Supplemental Table 1). SucT succinylates arabinogalactan and LAM, a modification that changes the structural properties of the mycomembrane (Palcekova et al., 2019). These data suggest that in cells deleted for *lamA*, in which the levels of PgfA and MmpL3 are lower, the presence of lipoglycans or their modifications become more important. In fact, we find that cells overexpressing PgfA, which results in more TDM (Fig. 3D), also have lower levels of cell-associated LAM (Fig. 4F).

Taken, together, our data suggest that PgfA and the presumed corynebacterial ortholog, Ncgl2760, do not have the same function. Further, our data uncover a previously unknown connection between TMM transport, or assembly of the mycomembrane, and LM/LAM. We find that the levels of LAM, and to a lesser extent LM, are negatively correlated with the levels of PgfA-mediated TMM-trafficking, suggesting that there may be competing pathways for the transport or synthesis of these molecules, a notion supported genetically by Tn-seq. Alternatively, altered PgfA-mediated TMM trafficking may lead to differences in LM/LAM accessibility to extraction methods.

**PgfA is necessary and sufficient for old pole growth in Δ*lamA* and the molecular requirements for growth between the poles are different**

347 As we have shown, PgfA and MmpL3 are necessary for polar growth (Fig.1A, 2D).

348 Additionally, in Δ*lamA* cells, which grow less from the old pole, PgfA and MmpL3 are less

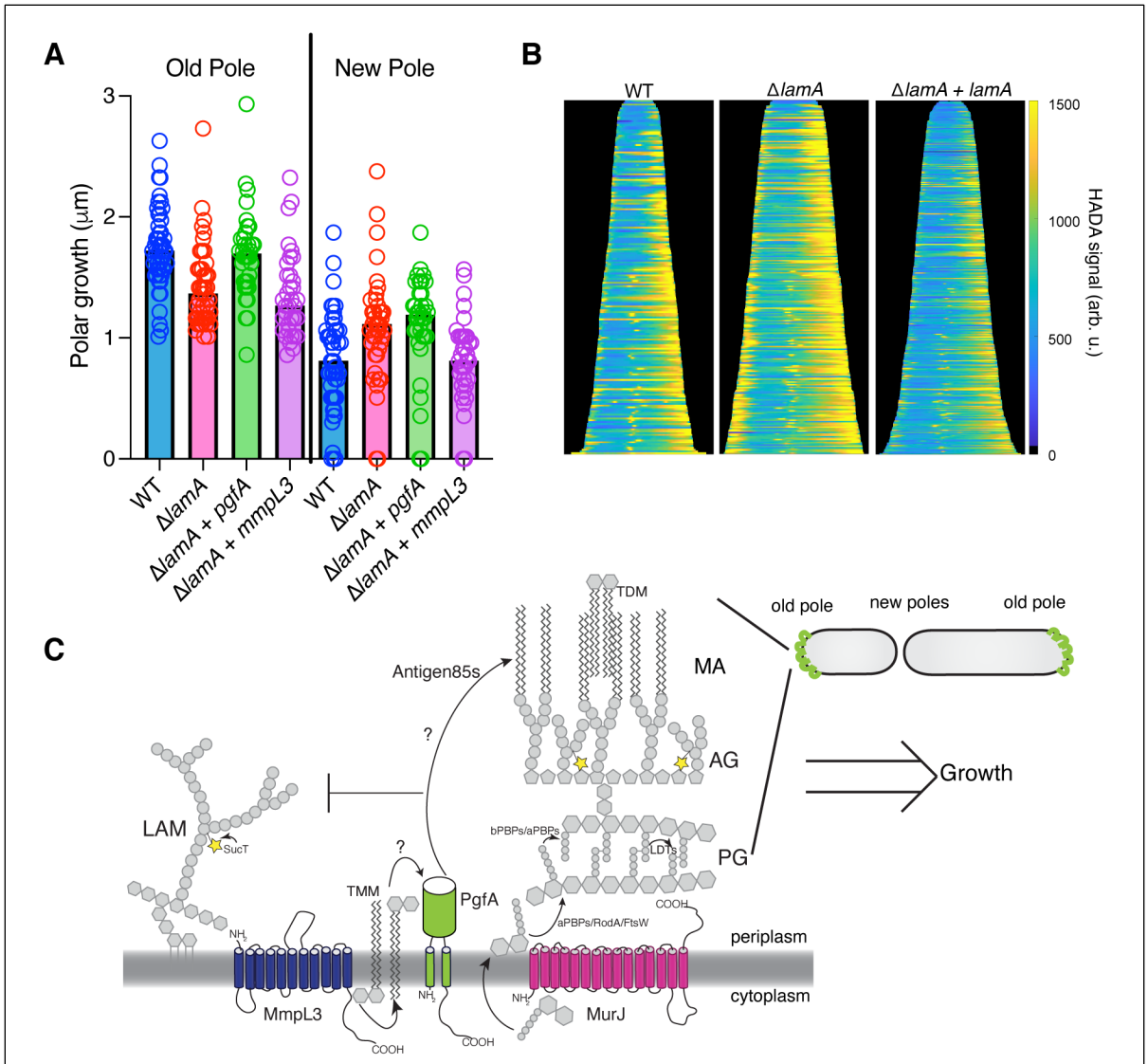


**Figure 5. PgfA is sufficient to restore old pole growth in Δ*lamA* cells. (A)** Cells were stained with amine-reactive dye, loaded into a microfluidic device, and imaged while perfusing dye-free media. By following the amount of unlabeled cell wall material, growth at the old and new poles was measured over time. The amount of growth incorporated per cell cycle is compared across WT cells, Δ*lamA* cells, and Δ*lamA* cells expressing a second copy of *pgfA* or *mmpL3* driven by a strong promoter**.** (N=51 WT; 44 Δ*lamA*; 36 Δ*lamA*+*pgfA;* 35 Δ*lamA*+*mmpL3*). Bars represent medians of the population. **(B)** Cells were stained with a fluorescent d-alanine analog, HADA, fixed, and imaged by fluorescence microscopy. MicrobeJ was used to segment the cells and measure intensity profiles along the long axis of the cell. Profiles were then aligned by the brightest pole and ordered by length as a proxy for cell cycle. (N=194 WT; N=259 Δ*lamA;* N=335 Δ*lamA*+*lamA)* **(C)** A model for asymmetric growth. PgfA is recruited by LamA to the old pole, where, together with other proteins, it functions to organize the mycobacterial cell envelope and promote fast cell elongation at one side of the cell.

349 abundant at this site (Fig. 2C). We wondered if loss of old pole growth in Δ*lamA* cells
350 could be directly attributed to the lowered abundance of either PgfA or MmpL3 at this site.
351 To test if PgfA and/or MmpL3 are sufficient to restore old pole growth in Δ*lamA*, we
352 created strains that expressed a second copy of these genes driven by a strong ribosomal
353 promoter. By quantifying polar growth with an established pulse-chase assay (Aldridge et
354 al., 2012; Rego et al., 2017), we find that Δ*lamA* cells encoding an extra copy of *pgfA*, but
355 not *mmpL3*, grow more from the old pole (Fig. 5A). These data suggest that the function
356 of PgfA or its interaction with other factors is necessary and sufficient for growth from the
357 old pole in *M. smegmatis*.

358 Intriguingly, overexpression of PgfA does not lead to more growth at the new pole
359 (Fig. 5A). This mirrors the observation that in Δ*lamA* cells - which grow more from the
360 new pole - neither MmpL3 nor PgfA are more abundant at this pole (Fig. 2C). Instead, the
361 levels of MurJ-msfGFP become increased (Figure 2 – figure supplement 2), leading us to
362 hypothesize that peptidoglycan synthesis increases at this site in the absence of *lamA*.
363 To test this, we stained cells with the fluorescent D-Ala analogue HADA, which is
364 incorporated into peptidoglycan through the cytoplasmic route of synthesis(García-
365 Heredia et al., 2018). In agreement with the increased MurJ abundance at the new pole,
366 we find that Δ*lamA* cells have increased HADA staining at the new pole (Fig. 5B). These
367 data suggest that the molecular requirements for growth between the new and old poles
368 may be different: with PgfA being rate limiting at the old pole and PG synthesis being rate
369 limiting at the new pole.

370

371 **DISCUSSION**

372 Our understanding of the mechanisms that govern polar growth and division are
373 at a nascent stage compared to our understanding of these processes in model rod
374 shaped bacteria (Baranowski et al., 2019; Kieser and Rubin, 2014). This is unfortunate
375 because the enzymes that create and remodel the cell envelope are a rich source of anti-
376 bacterial drug targets. In addition, the unusual mode of asymmetric polar growth - coupled
377 with the complexity of constructing the multi-layered mycobacterial cell envelope - means
378 that the details of growth and division in mycobacteria are almost certainly different from
379 laterally growing rod-shaped bacteria.

380 Here, we investigate the function of a mycobacterial specific factor LamA. We had
381 previously shown that LamA is, in part, responsible for asymmetric polar growth. Cells
382 missing LamA grow more symmetrically and are uniformly susceptible to several drugs
383 (Rego et al., 2017). How does LamA create asymmetry? We make inroads into answering
384 this question by investigating the cellular function of MSMEG_0317, another protein of
385 unknown function, which was predicted to interact with LamA. We show that
386 MSMEG_0317, renamed PgfA, is involved in the trafficking of mycolic acids in the
387 periplasmic space. PgfA interacts with a TMM analog, consistent with a role in directly
388 trafficking TMM. Additionally, our data point to a more global function for PgfA in
389 regulating the composition of the cell envelope. Specifically, we find that PgfA levels
390 negatively correlate with the abundance of LAM, and to some extent LM, two large and
391 abundant lipoglycans in the cell envelope. These data suggest that there may be
392 compensatory or competing mechanisms for the transport and/or synthesis of TMM and
393 LM/LAM (Fig. 5C). Further strengthening that argument, we find that Δ*lamA* cells, which
394 have less PgfA, are more reliant on SucT - an enzyme that succinylates LAM and

395 arabinogalactan (Bhamidi et al., 2008; Palcekova et al., 2019). It may be that TMM and
396 LM/LAM are simply competing for space in the outer leaflet of the mycomembrane.
397 However, to date, altered LM/LAM levels have not been reported for other TMM-trafficking
398 mutants, suggesting that there may be more active regulation controlling the levels or
399 transport of these two molecules. Indeed, others have speculated that succinylation itself
400 may act to negatively regulate mycoloylation, as succinylated arabinan chains are found
401 to be unmycoloylated (Bhamidi et al., 2008).

402 Deletion of *lamA* results in less PgfA and MmpL3 at one side of the cell, the 'old
403 pole', leading to less growth from that side of the cell. Increased expression of PgfA but
404 not MmpL3 restores growth at that side of the cell, suggesting that PgfA's role in
405 coordinating lipid trafficking, or the presence of the protein itself, is rate limiting for growth
406 at the old pole (Fig. 5C). Further research will be needed to understand how a TMM-
407 binding protein influences the rate of cell wall insertion at the old pole. Indeed, insertion
408 of new cell wall material requires the concerted effort of many synthetic enzymes,
409 including those that polymerize and crosslink peptidoglycan. In mycobacteria, the
410 bifunctional class A PBPs (aPBPs) are the dominant enzymes required for cell elongation.
411 In other organisms, aPBPs are activated by inner or outer membrane-anchored proteins
412 (Fenton et al., 2018; Paradis-Bleau et al., 2010; Typas et al., 2010), though no activator
413 of PonA1 - the major aPBP in mycobacteria - has been found. Thus, it is intriguing to
414 speculate that PgfA – a protein involved in mycomembrane precursor transport - may be
415 needed to activate PG synthesis at the old pole in mycobacteria.

416 What are the requirements for growth at the new pole – the pole newly formed by
417 division? In Δ*lamA*, this pole grows more without an increase in PgfA or MmpL3; instead,

418 enzymes involved in PG synthesis are more abundant at this site in Δ*lamA*. These
419 observations suggest that the requirements for growth between the two poles are
420 fundamentally different, at least for a certain time after the onset of pole elongation.
421 Indeed, new poles will eventually become old poles in the next round of division. We see
422 that PgfA and MmpL3 localize to the "new old poles" after division, establishing
423 asymmetry in the next generation. How does LamA affect the growth of the poles in
424 opposite directions – inhibiting one but activating another? Future research is needed,
425 but our data suggest that the new and old poles of mycobacteria may be distinct sites,
426 with different molecular factors and requirements for growth. Our results suggest that
427 LamA influences these differences to create asymmetry in individual cells, leading to a
428 heterogeneous population better able to survive certain stresses, like antibiotics.
429

430 **Acknowledgements**

431 We thank members of the Rego lab for helpful suggestions. This work was supported by
432 the National Institutes of Health, R01AI148255 to E.H.R, who was also supported by the
433 Searle and Pew Foundations. B.M.S. was supported by the National Science Foundation
434 (CAREER Award 1654408). C.W and J.L. were supported by the NIH grants
435 R01AI087946 and R01GM110243.
436
437

438 **Materials and Methods**

439

440 Table 1: Strains used in this study

| **Reagent type (species) or resource** | **Designation** | **Source or reference** | **Identifiers** | **Additional Information** |
|---|---|---|---|---|
| strain (*Mycobacterium smegmatis)* | | | *Mycobacterium smegmatis* mc$^2$155 | Wild type *M. smegmatis* |
| strain (*M. smegmatis)* | KG26 | this work | mc2155Δmsmeg_0317 L5::ptetO-msmeg_0317 | Parental swap strain |
| Strain ( *M. smegmatis*) | HR342 | Rego et al 2016 | mc2155ΔMSMEG_4265 | LamA knockout strain |
| strain (*M. smegmatis)* | KG97 | This work | mc2 155 Δmsmeg_0317 L5::ptetO-msmeg_0317-myc /pTetR | Strain used for the Anhydrotetracyline inducible depletion of PgfA |
| strain (*M. smegmatis)* | KG81 | This work | mc2 155 Δmsmeg_0317 pL5:pNative- msmeg_0317 -mRFP-myc | Strain used for determining PgfA localization |
| strain (*M. smegmatis)* | HR388 | Rego et al 2016 | mc2155 L5::pG-MCK-ptb21-egfp-wag31 tweety::ptb21-ftsZ-mCherry2B | Strain used to determine localization of FtsZ & Wag31 |
| strain (*M. smegmatis)* | CMG184 | This work | mc2155 tw:: ptb21 mmpL3$_{TB}$-msfGFP | Strain used to determine localization of MmpL3 |

| | | | | |
|---|---|---|---|---|
| strain (*M. smegmatis)* | CMG530 | This work | mc2155 Δ msmeg_0317 L5:: pTetO- msmeg_0317 -3X-Flag tw:: ptb21-mmpL3$_{TB}$-msfGFP | Strain used for co-immunoprecipitation of MmpL3 and PgfA |
| strain (*M. smegmatis)* | KG167 | This work | mc2155 Δ msmeg_0317 L5:: pTetO- msmeg_0317 -3X-Flag | Control strain used for co-immunoprecipitation of MmpL3 and PgfA |
| strain (*M. smegmatis)* | CMG184 | This work | mc2155 tw:: ptb21 mmpL3$_{TB}$-msfGFP | Strain used to determine localization of MmpL3 |
| strain (*M. smegmatis)* | CMG481 | This work | mc2155 ΔlamA::zeo L5:: pNative-lamA-strep tw:: ptb21 mmpL3$_{TB}$-msfGFP | Strain used to determine localization of MmpL3 in a ΔlamA background with LamA complemented under its native promoter |
| strain (*M. smegmatis)* | CMG557 | This work | mc2155 L5:: pTetO-MS0317-myc #1 | Strain used for measuring polar growth in a PgfA merodiploid background |
| strain (*M. smegmatis)* | KG175 | This work | mc2155 ΔlamA L5::pTetO-ms0317-myc | Strain used for measuring polar growth in a PgfA merodiploid and LamA knockout background |
| strain (*M. smegmatis)* | CMG585 | This work | mc2155 L5:: pTetO mmpL3$_{TB}$-myc | Strain used for measuring polar growth in an MmpL3 merodiploid background |
| strain (*M. smegmatis)* | CMG587 | This work | mc2155 ΔlamA L5:: pTetO mmpL3$_{TB}$-myc | Strain used for measuring polar growth in an MmpL3 merodiploid and LamA knockout background |
| strain (*M. smegmatis)* | KG154 | This work | mc2 155 ΔlamA Δmsmeg_0317 pL5:pNative- msmeg_0317 -mRFP-myc | Strain used for PgfA localization in LamA knockout background |

| | | | | |
|---|---|---|---|---|
| strain (*M. smegmatis)* | KG157 | This work | mc2 155 ∆lamA ∆msmeg_0317 pL5:pNative- msmeg_0317 -mRFP-myc pL5 pNative-lamA-strep | Strain used for PgfA localization in a background where lamA was complemented in LamA knockout |
| strain (*M. smegmatis)* | CMG206 | This work | mc2155 tw:: ptb21 msfGFP-MurJ$_{TB}$ | Strain used for localization of MurJ |
| strain (*M. smegmatis)* | CMG199 | This work | mc2155 ∆lamA tw:: ptb21 msfGFP-murJ$_{TB}$ | Strain used for localization of MurJ in a LamA knockout background |
| strain (*M. smegmatis)* | CMG485 | This work | mc2155 ∆lamA::zeo L5:: pNative LamA strep tw:: ptb21 msfGFP-MurJ$_{TB}$ | Strain used for localization of MurJ in a LamA knockout background where LamA was complemented under its native promoter |
| strain (*M. smegmatis)* | KG244 | This work | mc2 155 L5::pLJR962-mmpL3-sgRNA | CRISPR inducible MmpL3 depletion strain |
| strain (*M. smegmatis)* | KG289/ CMG549 | This work | mc2 155 L5::pLJR962-msmeg_0317-sgRNA:: pTweety-pNative-msmeg_0315 | CRISPR inducible PgfA depletion strain |
| strain (*M. smegmatis)* | KG47 | This work | mc2 155 ∆msmeg_0317 L5::pTetO-msmeg_0317-mGFPmut3-myc | C-terminal GFP tagged PgfA strain |
| Strain (*M. smegmatis*) | KG73 | This work | mc2 155 ∆msmeg_0317 L5:: pTetO-mGFP-mut3-MS0317-myc | N-terminal GFP tagged PgfA strain |
| Strain (*M. smegmatis*) | KG167 | This work | mc2 155 ∆msmeg_0317 L5:: pTetO-MS0317-3XFLAG | Strain carrying MSMEG_0317-3X-FLAG, used for TMM pulldown |

| | | | | |
|---|---|---|---|---|
| Strain (*M. smegmatis*) | KG60 | This work | mc2 155 /pTetOR-msmeg_0317-myc | Strain carrying tetracycline inducible over-expression plasmid for PgfA |
| Strain (*M. smegmatis*) | KG286 | This work | mc2 155 Δmsmeg_0317 L5:: pTetO-msmeg ΔC | Strain carrying msmeg_0317 without c-terminal cytoplasmic tail |
| Plasmid (*E. coli*) | KG147 | This work | DH5 α /pL5-pTetO-*Ncgl2760*-myc | Plasmid carrying corynebacterial *ncgl2760* gene |
| Plasmid (*E. coli*) | KG284 | This work | DH5 α /pL5-pTetO-*Ncgl2760*-msmeg_0317-C-term | Plasmid carrying corynebacterial *ncgl2760* gene fused to cytosolic C-terminal of *msmeg_0317* gene |
| Plasmid (*E. coli*) | CMG541 | This work | Dh5a / pTweety pNative Msm_0315-strep | Plasmid carrying mycobacterial gene MSMEG_0315 with a C-terminal strep tag |

441

442

443 **Bacterial strains and culture conditions**: *M. smegmatis* mc$^2$155 was grown in
444 Middlebrook 7H9 broth supplemented with 0.05% Tween80, 0.2% glycerol, 5 gm/L
445 albumin, 2 gm/L dextrose and 0.003 gm/L catalase or plated on LB agar. *Escherichia coli*
446 DH5α cells were grown in LB broth or on LB agar plates. Concentrations of antibiotics
447 used for *M. smegmatis* is as follows: 20 μg/ml zeocin, 25 μg/ml kanamycin, 50 μg/ml
448 hygromycin, and 20 μg/ml nourseothricin. Concentrations of antibiotics used for *E. coli*
449 used for *E. coli* is as follows: 40 μg/ml zeocin, 50 μg/ml kanamycin, 100 μg/ml hygromycin,
450 and 40 μg/ml nourseothricin.

451 **Plasmid and strain construction**: Strains used in this study are listed in Table 1.
452 Oligos and primers are listed in Supplemental Table 2. In brief, before deleting the native
453 copy of *msmeg_0317*, a merodiploid strain was created by inserting a second copy of
454 *msmeg_0317* gene under pTetO promoter using a $Kan^R$ L5 integrating vector.
455 Subsequently, in the merodiploid strain, an in-frame deletion was made by replacing the
456 native copy of *msmeg_0317 gene* with a zeocin resistance cassette flanked by loxP sites
457 using recombineering (van Kessel and Hatfull, 2007). *msmeg_0317* and its variants,
458 including the fluorescent protein fusions, were cloned in a $Nat^R$ L5 integrating vector for
459 allele exchange at the L5 site. The *msmeg_0317* depletion strain was made by
460 transforming an episomal $Hyg^R$ marked vector constitutively expressing TetR repressor
461 into a strain expressing a single copy of *msmeg_0317* controlled by the pTetO promoter.
462 For expression of *msmeg_0317* driven by the native promoter, 200bp upstream of
463 msmeg_0317 chromosomal locus was used. For the MmpL3 and MurJ fluorescent
464 fusions and co-IP experiments, the genes were cloned from the *M. tuberculosis* genome,
465 expressed from the ptb21 promoter and integrated in single copy at the tweety phage
466 integration site. All plasmid constructs were made using isothermal Gibson assembly
467 whereby insert and vector backbone shared 20-25 bp of homology.

468 **MSMEG_0317 Depletion:**

469 *Promoter depletion.* To transcriptionally deplete *msmeg_0317* in Msm, the ATC-inducible
470 Tet-ON system was used. The only copy of *msmeg_0317* was driven by the pTetO
471 promoter, while the TetR repressor was constitutively expressed in trans from an
472 episomal vector. MSMEG_0317 was depleted by removing ATC from the medium and
473 cells were grown for 18 hours. Subsequently, MSMEG_0317 depleted cells were re-

474 diluted in fresh medium, also without ATC, and samples at different timepoints were taken
475 and processed for cyro-electron microscopy. Alternatively, to avoid changes in LM/LAM
476 abundance that have been found to correlated with cell density and growth phase (21),
477 at 18 hours of depletion, half of the culture was removed for lipid extraction and analysis,
478 and replaced with fresh media. Lipid analysis was performed at timepoints before and
479 after the decrease in OD indicating cessation of growth (Fig. S3).
480 *CRISPRi depletion.* To transcriptionally deplete *mmpL3* and *msmeg_0317* using
481 CRISPRi, both dCas9 and the respective guide RNAs were cloned in an L5 integrating
482 plasmid pIJR962 (Rock et al., 2017). The CRISPRi silencing of *mmpL3/msmeg_0317* was
483 induced by adding ATC to a final concentration of 100 ng/ul. The induction was carried
484 out for the indicated timepoints.
485 **Time-lapse and fluorescence microscopy**: An inverted Nikon Ti-E microscope
486 was used for the time-lapse imaging. An environmental chamber (Okolabs) was
487 maintained at 37°C. Cells were cultivated in an B04 microfluidics plate from CellAsic,
488 continuously supplied with fresh medium, and imaged every 15 minutes using a 60x 1.4
489 N.A. Plan Apochromat phase contrast objective (Nikon). Fluorescence was excited using
490 the Spectra X Light Engine (Lumencor), separated using single- or multi- wavelength
491 dichroic mirrors, filtered through single bandpass emission filters, and detected with an
492 sCMOS camera (ORCA Flash 4.0). Filters are: GFP (Ex: 470/24; Em: 515/30 or 525/50);
493 mRFP (Ex: 550/15; Em: 595/44 or 630/75). To reduce phototoxicity exposure times were
494 kept below 100ms for excitation with 470nm and 300ms for excitation with 550nm.
495 **Kymograph analysis and Image analysis.** Time-lapse images were analyzed in
496 open-source image analysis software Fiji (30) and a custom MATLAB program was used

497 to generate kymographs. Source code will be uploaded to Github. Specifically, for a single
498 cell, in Fiji, a 5-pixel wide segmented line was drawn from the new pole to the old pole at
499 each time point during the cell cycle. This was repeated on 20-50 cells. These line profiles
500 were then imported into MATLAB, where a custom script was used to generate an
501 average kymograph by 2D interpolation of the individual kymographs. For the
502 demographs shown in Fig 5, cells were segmented and intensity profiles measured using
503 MicrobeJ. Output intensity profiles were then transferred to Matlab, sorted by cell length,
504 and aligned by the brightest pole for visualization.

505 **N-x-AlkTMM-C15 mediated protein capture:**

506 *Preparation of cell lysate. M. smegmatis* expressing 3x FLAG-tagged
507 MSMEG_0317 starter culture was generated by inoculating a single colony from a freshly
508 streaked LB agar plate supplemented with zeocin and nourseothricin (20 ug/ml each) into
509 10 ml liquid 7H9 medium in a sterile culture tube. The starter culture was grown until mid-
510 logarithmic phase and then diluted to OD600 0.2 with 7H9 medium to a final volume of
511 80 ml. The culture was split into two equal volumes in 125ml sterilized culture flasks. To
512 one flask, N-x-AlkTMM-C15 was added to a final concentration of 100 μM with (final
513 DMSO concentration of 2%), while the other flask was left untreated as a DMSO control
514 (final DMSO concentration of 2%). Both flasks were incubated with shaking until OD600
515 0.8 was reached. The cells were pelleted by centrifugation at 6,500 xg at 4 °C for 10 min.
516 The cell pellets were washed twice with PBS, re-suspended in 6 ml PBS, and split into
517 two equal volumes. One aliquot was exposed to UV irradiation for 30 min with a 5-watt
518 365 nm UV bench lamp (UVP) while the other was left unexposed as a control. The cell
519 pellets were collected by centrifugation and re-suspended in 600 μl lysis buffer (2 mg/ml

520 lysozyme, 1 mM phenylmethylsulfonyl fluoride (PMSF) in 1x PBS), transferred to
521 scintillation vials, and incubated at 37 °C for 2 h. The mixtures were transferred to 1.5 ml
522 screw-cap vials containing 0.25 ml of 0.1 mm zirconia/silica beads (BioSpec Products)
523 and subjected to bead beating 3x for 1 min each using a FastPrep-24 bead beater (MP
524 Biomedicals). The lysate was transferred to a scintillation vial, then SDS was added to a
525 final concentration of 2% from a 20% SDS stock. Cell extracts were incubated at 60 °C
526 for 2 h with constant stirring. The lysates were transferred to microcentrifuge tubes and
527 centrifuged at 3,200 xg for 10 min at 4 °C. The supernatant was collected and stored in
528 separate tubes at 4 °C until use.

529 CuAAC and affinity enrichment. To reduce SDS concentration, 500 μl of
530 methanol/chloroform (2:1 v/v) was added to 184 μl of cell lysate. The resulting protein
531 precipitate was centrifuged at 18,000 xg at 4 °C for 10 minutes and the supernatant was
532 discarded. The precipitate was air dried and solubilized using 184 μl of 0.5% SDS/0.05%
533 LDAO buffer. Copper catalyzed azide-alkyne cycloaddition (CuAAC) was carried out by
534 sequential addition of 1 mM AzTB (azido-TAMRA-biotin (4 μl), Click Chemistry Tools), 60
535 mM sodium ascorbate (4 μl), 6.4 mM TBTA ligand (4 μl), and 50 mM copper sulfate (4 μl)
536 to give a final volume of 200 μl. The final reagent concentration was 20 μM AzTB; 1.2 mM
537 sodium ascorbate; 128 μM TBTA; and 1 mM copper(II) sulfate. The mixture was
538 thoroughly mixed by pipetting up and down and the reaction was incubated for 2 h in the
539 dark with constant agitation at 37 °C. Excess AzTB was removed by precipitating proteins
540 in methanol/chloroform (2:1 v/v), discarding supernatant, and solubilizing protein pellets
541 in 200 μl 0.5% SDS/0.05% LDAO buffer as described above. Protein concentration was
542 determined by Bradford assay. 15 μl of each sample was saved as input sample. The

543 remaining sample was mixed with 40 μl Pierce avidin-agarose beads (ThermoFisher
544 Scientific) that had been pre-washed 3x with 0.5% SDS/0.05% LDAO buffer (100 μl). The
545 bead mixture was incubated at room temperature with constant rotation for 2 h. The beads
546 were washed 3x with 0.5% SDS/0.05% LDAO buffer (100 μl) followed by 3x with PBS
547 (100 μl) with centrifugation at 1,000 xg for 1 min between each wash. Bound proteins
548 were eluted by boiling at 95 °C for 15 min in 30 μl of 4x sample buffer.

549 SDS-PAGE and Western blot. 5 μg of input and 10 μl of output was resolved by
550 SDS-PAGE by 4-20% acrylamide gels and analyzed by in-gel fluorescence using a
551 Typhoon FLA 7000 (GE Healthcare Life Science) using the rhodamine channel to detect
552 TAMRA-labeled proteins.

553 The gel was fixed for 15 min (40% ethanol and 10% acetic acid in DI water), rinsed
554 3x with DI water 10 minutes each and stained overnight with agitation in QC colloidal
555 Coomassie stain (Bio-Rad). The gel was rinsed with DI water 3x for 10 min and imaged
556 using a ChemiDoc Touch Imaging System (Bio-Rad) and processed by Image Lab
557 software (Bio-Rad).

558 The above conditions were used to generate samples for Western blot analysis. 5
559 μg input controls and 10 μl eluted proteins were resolved by SDS-PAGE. After gel
560 electrophoresis, proteins were transferred onto an Immun-Blot PVDF membrane (Bio-
561 Rad). The PVDF membrane was equilibrated in ethanol and blotting filter paper
562 (ThermoFisher Scientific) was equilibrated in transfer buffer (25 mM Tris, 193 mM glycine,
563 and 20% ethanol) before placement in a transfer cassette. Proteins were transferred
564 electrophoretically at a constant voltage of 25 V for 7 min using a Trans-Blot Turbo
565 Transfer System (Bio-Rad). After transfer, the membrane was blocked overnight at 4 °C

566 in 5% dry milk in Tris-buffered saline containing Tween 20, pH 7.6 (50 mM Tris, 0.5 M
567 NaCl, 0.02% Tween 20 (TBST)). Anti-FLAG-HRP (ThermoFisher Scientific) was used at
568 1:1,000 dilution using 2% dry milk in TBST. The membrane was incubated with antibody
569 at 4 °C overnight with constant rocking. The membrane was washed 3x for 10 min each
570 with TBST. The membrane was treated with SuperSignal West Pico PLUS
571 chemiluminescent reagent (ThermoFisher Scientific) and chemiluminescence was
572 detected on a ChemiDoc Touch Imaging system (Bio-Rad).

573 **Tn-seq.** Transposon libraries in wild type and Δ*lamA* (HR342) were prepared as
574 and sequenced described elsewhere (Dragset et al., 2019). This was done independently
575 on two separate days for a total of two biological replicates in each strain. The TRANSIT
576 and TPP python packages were used to map insertions to the $mc^2155$ genome and
577 quantitatively compare insertions across stains, using the 'resampling' option (DeJesus,
578 Michael A. et al., 2015).

579 **Co-immunoprecipitation:**

580 Mycobacterial cultures were grown to mid-log phase as described above. Protocol for
581 crosslinking was adapted from Belardinelli et al, Sci Rep, 2019 (Belardinelli et al., 2019).
582 Cells were washed with 1x phosphate buffered saline (PBS) once. Pellets were
583 resuspended in 1mL of 1x PBS with 1.25mM dithiobis (succinimidyl propionate) (DSP)
584 and incubated for 30 minutes at 37˚C for crosslinking. After incubation, cells were pelleted
585 at 10,000xg for 5 minutes at room temperature and the supernatant was discarded. The
586 pellet was resuspended in lysis buffer (50mM Tris-HCl, pH 7.4; 150mM NaCl; 10ug/mL
587 DNase I; one tablet Roche cOmplete EDTA free protease inhibitor cocktail; and and 0.5%
588 Igepal Nonidet P40 Substitute) and lysed with a BeadBug™ Microtube Homogenizer at

589 4,000rpm six times for 30 seconds each, icing in between. Lysed cells were spun down
590 at 15,000xg for 15 minutes at 4˚C, and the supernatant was transferred to a clean
591 eppendorf tube. Lysates were incubated, where indicated, with either GFP-Trap Magnetic
592 Agarose (Chromotek) or magnetic a-FLAG M2 beads (Sigma-Aldrich) and incubated at
593 4˚C overnight, rotating. After incubation, samples were spun down at 2,500xg for 1 minute
594 at room temperature and flow through was discarded. Beads were washed three times
595 with non-detergent wash buffer (10mM Tris-HCl, pH 7.4; 150mM NaCl, 0.5mM EDTA).
596 GFP-Trap samples were eluted with 2x Laemmli Buffer (Bio-Rad) prepared with 50mM
597 (DTT) and boiled at 95˚C for 5 minutes. FLAG M2 beads were eluted twice with 3xFLAG
598 peptide (Sigma-Aldrich) for 30 minutes rotating at 4˚C. All samples not already treated
599 with Laemmli Buffer + DTT were prepared for western blotting by addition of Laemmli
600 Buffer + DTT and boiled at 95˚C for 5 minutes, to reverse all crosslinks.

601 *Western blot verification*

602 Samples were run on NuPAGE™ (Thermo Fisher) 4-12% Bis-Tris gels in 1x MOPS-SDS
603 running buffer. Proteins were transferred to nitrocellulose membranes and probed with
604 1:1,000 a-FLAG primary (Sigma-Aldrich, clone M2) and 1:5,000 a-mouse secondary
605 (Thermo Fisher, Superclonal™ A28177). SuperSignal™ West Femto Extended Duration
606 Substrate (Thermo Fisher) was used for chemiluminescent visualization on an Amersham
607 ImageQuant 800 system.

608 **Lipid extraction and analysis.**

609 *TMM/TDM.* Crude lipids were extracted from equal wet cell pellet weights of the
610 either *mmpL3* depletion or *msmeg_0317* depleted cells after 9,12, and 15 hours with or
611 without ATC with 2:1 chloroform/methanol mixture for 12 hours. The organic layer was

612 separated from the cell debris centrifugation at 4000g. The organic extract was air dried
613 overnight. The dried extract was dissolved in 50 μl of 2:1 chloroform/methanol. TMMs and
614 TDMs were separated on by high performance thin layer chromatography (HPTLC) (Silica
615 gel 60, EMD Merck) using chloroform/methanol/ water (25:4:9:0.4). TMMs/TDMs were
616 visualized by spraying the TLC sheet with 20% 1-napthaol in 5% sulfuric acid and charring
617 the plate at 110°C Trehalose containing lipids (TMMs/TDMs) appear as purple bands
618 after charring.

619 *LM/LAM.* Extraction, purification and analysis of lipids were as described
620 previously (Rahlwes et al., 2019). Briefly, crude lipids were extracted from equal wet cell
621 pellet weights of the MSMEG_0317 depletion strains after 18, 24, 27, 30, and 33 hrs with
622 or without ATC. After lipid extraction using chloroform/methanol, LM and LAM were
623 extracted from the delipidated pellet by incubation with phenol/water (1:1) for 2 hrs at
624 55°C. Phospholipids and PIMs extracted by chloroform/methanol were further purified by
625 *n*-butanol/water phase partitioning, and separated by high performance thin layer
626 chromatography (HPTLC) (Silica gel 60, EMD Merck) using chloroform/methanol/ 13 M
627 ammonia/1 M ammonium acetate/ water (180:140:9:9:23). Phospholipids were visualized
628 via cupric acetate staining. PIMs were visualized with orcinol staining as described(Sena
629 et al., 2010). LM/LAM samples were separated by SDS-PAGE (15% gel) and visualized
630 using ProQ Emerald 488 glycan staining kit (Life Technologies). To detect LM/LAM in
631 culture supernatants, the supernatants were initially treated with a final concentration of
632 50 μg/ml Proteinase K for 4 hours at 50°C. The treated supernatants were
633 electrophoresed on 15% SDS-PAGE. LM/LAM were blotted onto nitrocellulose at 20 V
634 for 45 minutes using semi-dry transfer method. Post-transfer, the membrane was blocked

635 by 5% milk in Tris-buffered saline supplemented with 0.05% Tween-20 (TBST). The
636 blocked membrane was then probed overnight with CS-35 antibody (BEI Resources, NIH)
637 at 1:250 dilution at 4°C. The membrane was washed with TBST five times for five minutes
638 each. Post-washing, it was probed with anti-mouse secondary for one hour at room
639 temperature. Membrane was then washed five times for five minutes with TBST. Thermo
640 Scientific's west dura chemiluminescent reagent was used to develop the membrane.

641 **Sample preparation and image collection for Cryo-EM.** Wild type and
642 MSMEG_0317 depleted *M. smegmatis* cells were pelleted, washed twice with 1X
643 phosphate buffered saline (PBS), and suspended in ~20µl PBS. The culture was
644 subsequently deposited onto freshly glow-discharged holey carbon grids. The grids were
645 then blotted with filter paper manually for about 4 seconds and rapidly frozen in liquid
646 ethane. The frozen grids were transferred into a 300kV Titan Krios electron microscope
647 (ThermoFisher Scientific) equipped with a K2 Summit direct detector and a quantum
648 energy filter (Gatan, Pleasanton, CA). Cryo-EM movie stacks were collected using
649 SerialEM (Mastronarde, 2005). MotionCor2 (Zheng et al., 2017) was used for drift
650 correction of the cryo-EM movie stacks. The grey levels of each micrograph are obtained
651 using MATLAB.

652 **Experimental Replicates.** Biological replicates are defined as independent
653 cultures grown in parallel or on separate days. Technical replicates are defined at the
654 same culture, measured independently. All the experiments were performed at least
655 twice - often three or more times - with biological replicates.

656 **Data and Materials Availability.** Data generated in this study are included in the
657 manuscript and supporting files. Request for strains can be addressed to the
658 corresponding author: hesper.rego@yale.edu
659

660 Reference List


661 Abdali, N., Younas, F., Mafakheri, S., Pothula, K.R., Kleinekathöfer, U., Tauch, A., and
662 Benz, R. (2018). Identification and characterization of smallest pore-forming protein in
663 the cell wall of pathogenic Corynebacterium urealyticum DSM 7109. BMC Biochem *19,*
664 3.
665 Adams, O., Deme, J.C., Parker, J.L., CRyPTIC Consortium, Fowler, P.W., Lea, S.M.,
666 and Newstead, S. (2021). Cryo-EM structure and resistance landscape of M.
667 tuberculosis MmpL3: An emergent therapeutic target. Structure *29,* 1182-1191.e4.
668 Aldridge, B.B., Fernandez-Suarez, M., Heller, D., Ambravaneswaran, V., Irimia, D.,
669 Toner, M., and Fortune, S.M. (2012). Asymmetry and aging of mycobacterial cells lead
670 to variable growth and antibiotic susceptibility. Science *335,* 100-104.
671 Backus, K.M., Dolan, M.A., Barry, C.S., Joe, M., McPhie, P., Boshoff, H.I.M., Lowary,
672 T.L., Davis, B.G., and Barry, C.E. (2014). The Three Mycobacterium tuberculosis
673 Antigen 85 Isoforms Have Unique Substrates and Activities Determined by Non-active
674 Site Regions. J Biol Chem *289,* 25041-25053.
675 Baranowski, C., Rego, E.H., and Rubin, E.J. (2019). The Dream of a Mycobacterium.
676 Microbiol. Spectr. *7,* 10.1128/microbiolspec.GPP3-2018.
677 Belardinelli, J.M., Stevens, C.M., Li, W., Tan, Y.Z., Jones, V., Mancia, F., Zgurskaya,
678 H.I., and Jackson, M. (2019). The MmpL3 interactome reveals a complex crosstalk
679 between cell envelope biosynthesis and cell elongation and division in mycobacteria.
680 Sci. Rep. *9,* 10728-8.
681 Bhamidi, S., Scherman, M.S., Rithner, C.D., Prenni, J.E., Chatterjee, D., Khoo, K.H.,
682 and McNeil, M.R. (2008). The identification and location of succinyl residues and the
683 characterization of the interior arabinan region allow for a model of the complete primary
684 structure of Mycobacterium tuberculosis mycolyl arabinogalactan. J. Biol. Chem. *283,*
685 12992-13000.
686 Bosch, B., DeJesus, M.A., Poulton, N.C., Zhang, W., Engelhart, C.A., Zaveri, A.,
687 Lavalette, S., Ruecker, N., Trujillo, C., Wallach, J.B.*, et al.* (2021). Genome-wide gene
688 expression tuning reveals diverse vulnerabilities of M. tuberculosis. Cell *184,* 4579-
689 4592.e24.
690 Cashmore, T.J., Klatt, S., Yamaryo-Botte, Y., Brammananth, R., Rainczuk, A.K.,
691 McConville, M.J., Crellin, P.K., and Coppel, R.L. (2017). Identification of a Membrane
692 Protein Required for Lipomannan Maturation and Lipoarabinomannan Synthesis in
693 Corynebacterineae. J. Biol. Chem. *292,* 4976-4986.
694 Chiaradia, L., Lefebvre, C., Parra, J., Marcoux, J., Burlet-Schiltz, O., Etienne, G., Tropis,
695 M., and Daffé, M. (2017). Dissecting the mycobacterial cell envelope and defining the
696 composition of the native mycomembrane. Scientific Reports *7,* 12807-12.
697 Degiacomi, G., Benjak, A., Madacki, J., Boldrin, F., Provvedi, R., Palù, G., Kordulakova,
698 J., Cole, S.T., and Manganelli, R. (2017). Essentiality of mmpL3 and impact of its
699 silencing on Mycobacterium tuberculosis gene expression. Scientific Reports *7,* 43495.
700 DeJesus, M.A., Gerrick, E.R., Xu, W., Park, S.W., Long, J.E., Boutte, C.C., Rubin, E.J.,
701 Schnappinger, D., Ehrt, S., Fortune, S.M., Sassetti, C.M., and Ioerger, T.R. (2017).
702 Comprehensive Essentiality Analysis of the Mycobacterium tuberculosis Genome via
703 Saturating Transposon Mutagenesis. MBio *8,* 10.1128/mBio.02133-16.

DeJesus, M.A., Ambadipudi, C., Baker, R., Sassetti, C., and Ioerger, T.R. (2015). TRANSIT - A Software Tool for Himar1 TnSeq Analysis. PLOS Computational Biology *11,* e1004401.

Dragset, M.S., Ioerger, T.R., Zhang, Y.J., Mærk, M., Ginbot, Z., Sacchettini, J.C., Flo, T.H., Rubin, E.J., and Steigedal, M. (2019). Genome-wide Phenotypic Profiling Identifies and Categorizes Genes Required for Mycobacterial Low Iron Fitness. Sci Rep *9,*

Fay, A., Czudnochowski, N., Rock, J.M., Johnson, J.R., Krogan, N.J., Rosenberg, O., and Glickman, M.S. (2019a). Two Accessory Proteins Govern MmpL3 Mycolic Acid Transport in Mycobacteria. mBio *10,* 10.1128/mBio.00850-19.

Fay, A., Czudnochowski, N., Rock, J.M., Johnson, J.R., Krogan, N.J., Rosenberg, O., and Glickman, M.S. (2019b). Two Accessory Proteins Govern MmpL3 Mycolic Acid Transport in Mycobacteria. mBio *10,* 10.1128/mBio.00850-19.

Fenton, A.K., Manuse, S., Flores-Kim, J., Garcia, P.S., Mercy, C., Grangeasse, C., Bernhardt, T.G., and Rudner, D.Z. (2018). Phosphorylation-dependent activation of the cell wall synthase PBP2a in Streptococcus pneumoniae by MacP. Proceedings of the National Academy of Sciences - PNAS *115,* 2812-2817.

García-Heredia, A., Pohane, A.A., Melzer, E.S., Carr, C.R., Fiolek, T.J., Rundell, S.R., Lim, H.C., Wagner, J.C., Morita, Y.S., Swarts, B.M., and Siegrist, M.S. (2018). Peptidoglycan precursor synthesis along the sidewall of pole-growing mycobacteria. eLife *7,* e37243.

Hoffmann, C., Leis, A., Niederweis, M., Plitzko, J.M., and Engelhardt, H. (2008). Disclosure of the mycobacterial outer membrane: cryo-electron tomography and vitreous sections reveal the lipid bilayer structure. Proc. Natl. Acad. Sci. U. S. A. *105,* 3963-3967.

Jackson, M. (2014). The mycobacterial cell envelope-lipids. Cold Spring Harb Perspect. Med. *4,* 10.1101/cshperspect.a021105.

Jankute, M., Cox, J.A., Harrison, J., and Besra, G.S. (2015). Assembly of the Mycobacterial Cell Wall. Annu. Rev. Microbiol. *69,* 405-423.

Jumper, J., Evans, R., Pritzel, A., Green, T., Figurnov, M., Ronneberger, O., Tunyasuvunakool, K., Bates, R., Žídek, A., Potapenko, A.*, et al.* (2021). Highly accurate protein structure prediction with AlphaFold. Nature *596,* 583.

Kavunja, H.W., Biegas, K.J., Banahene, N., Stewart, J.A., Piligian, B.F., Groenevelt, J.M., Sein, C.E., Morita, Y.S., Niederweis, M., Siegrist, M.S., and Swarts, B.M. (2020). Photoactivatable Glycolipid Probes for Identifying Mycolate-Protein Interactions in Live Mycobacteria. J. Am. Chem. Soc. *142,* 7725-7731.

Kieser, K.J., and Rubin, E.J. (2014). How sisters grow apart: mycobacterial growth and division. Nat. Rev. Microbiol. *12,* 550-562.

Kilburn, J.O., and Takayama, K. (1981). Effects of ethambutol on accumulation and secretion of trehalose mycolates and free mycolic acid in Mycobacterium smegmatis. Antimicrob. Agents Chemother. *20,* 401-404.

La Rosa, V., Poce, G., Canseco, J.O., Buroni, S., Pasca, M.R., Biava, M., Raju, R.M., Porretta, G.C., Alfonso, S., Battilocchio, C.*, et al.* (2012). MmpL3 is the cellular target of the antitubercular pyrrole derivative BM212. Antimicrob. Agents Chemother. *56,* 324-331.

749 Lewis, J.A., and Hatfull, G.F. (2000). Identification and characterization of
750 mycobacteriophage L5 excisionase. Mol. Microbiol. *35,* 350-360.
751 Martini, M.C., Zhou, Y., Sun, H., and Shell, S.S. (2019). Defining the Transcriptional and
752 Post-transcriptional Landscapes of Mycobacterium smegmatis in Aerobic Growth and
753 Hypoxia. Front Microbiol *10,*
754 Mastronarde, D.N. (2005). Automated electron microscope tomography using robust
755 prediction of specimen movements. J Struct Biol *152,* 36-51.
756 Mikusova, K., Slayden, R.A., Besra, G.S., and Brennan, P.J. (1995). Biogenesis of the
757 mycobacterial cell wall and the site of action of ethambutol. Antimicrob. Agents
758 Chemother. *39,* 2484-2489.
759 Palcekova, Z., Angala, S.K., Belardinelli, J.M., Eskandarian, H.A., Joe, M., Brunton, R.,
760 Rithner, C., Jones, V., Nigou, J., Lowary, T.L*., et al.* (2019). Disruption of the SucT
761 acyltransferase in Mycobacterium smegmatis abrogates succinylation of cell envelope
762 polysaccharides. J. Biol. Chem. *294,* 10325-10335.
763 Paradis-Bleau, C., Markovski, M., Uehara, T., Lupoli, T.J., Walker, S., Kahne, D.E., and
764 Bernhardt, T.G. (2010). Lipoprotein Cofactors Located in the Outer Membrane Activate
765 Bacterial Cell Wall Polymerases. Cell *143,* 1110-1120.
766 Pashley, C.A., and Parish, T. (2003). Efficient switching of mycobacteriophage L5-
767 based integrating plasmids in Mycobacterium tuberculosis. FEMS Microbiology Letters
768 *229,* 211-215.
769 Patel, O., Brammananth, R., Dai, W., Panjikar, S., Coppel, R.L., Lucet, I.S., and Crellin,
770 P.K. (2022). Crystal structure of the putative cell-wall lipoglycan biosynthesis protein
771 LmcA from Mycobacterium smegmatis. Acta Crystallogr. D. Struct. Biol. *78,* 494-508.
772 Rahlwes, K.C., Puffal, J., and Morita, Y.S. (2019). Purification and Analysis of
773 Mycobacterial Phosphatidylinositol Mannosides, Lipomannan, and Lipoarabinomannan.
774 In Bacterial Polysaccharides: Methods and Protocols, Brockhausen, Inka ed., (New
775 York, NY: Springer New York) pp. 59-75.
776 Rego, E.H., Audette, R.E., and Rubin, E.J. (2017). Deletion of a mycobacterial divisome
777 factor collapses single-cell phenotypic heterogeneity. Nature *546,* 153-157.
778 Richardson, K., Bennion, O.T., Tan, S., Hoang, A.N., Cokol, M., and Aldridge, B.B.
779 (2016). Temporal and intrinsic factors of rifampicin tolerance in mycobacteria. Proc.
780 Natl. Acad. Sci. U. S. A. *113,* 8302.
781 Rock, J.M., Hopkins, F.F., Chavez, A., Diallo, M., Chase, M.R., Gerrick, E.R., Pritchard,
782 J.R., Church, G.M., Rubin, E.J., Sassetti, C.M., Schnappinger, D., and Fortune, S.M.
783 (2017). Programmable transcriptional repression in mycobacteria using an orthogonal
784 CRISPR interference platform. Nat. Microbiol. *2,* 16274.
785 Sena, C.B.C., Fukuda, T., Miyanagi, K., Matsumoto, S., Kobayashi, K., Murakami, Y.,
786 Maeda, Y., Kinoshita, T., and Morita, Y.S. (2010). Controlled Expression of Branch-
787 forming Mannosyltransferase Is Critical for Mycobacterial Lipoarabinomannan
788 Biosynthesis. J Biol Chem *285,* 13326-13336.
789 Soltan Mohammadi, N., Mafakheri, S., Abdali, N., Bárcena-Uribarri, I., Tauch, A., and
790 Benz, R. (2013). Identification and characterization of the channel-forming protein in the
791 cell wall of Corynebacterium amycolatum. Biochimica Et Biophysica Acta (BBA) -
792 Biomembranes *1828,* 2574-2582.

Su, C.C., Klenotic, P.A., Cui, M., Lyu, M., Morgan, C.E., and Yu, E.W. (2021). Structures of the mycobacterial membrane protein MmpL3 reveal its mechanism of lipid transport. PLoS Biol. *19,* e3001370.

Su, C., Klenotic, P.A., Bolla, J.R., Purdy, G.E., Robinson, C.V., and Yu, E.W. (2019). MmpL3 is a lipid transporter that binds trehalose monomycolate and phosphatidylethanolamine. Proceedings of the National Academy of Sciences - PNAS *116,* 11241-11246.

Tahlan, K., Wilson, R., Kastrinsky, D.B., Arora, K., Nair, V., Fischer, E., Barnes, S.W., Walker, J.R., Alland, D., Barry, C.E., and Boshoff, H.I. (2012). SQ109 Targets MmpL3, a Membrane Transporter of Trehalose Monomycolate Involved in Mycolic Acid Donation to the Cell Wall Core of Mycobacterium tuberculosis. Antimicrob Agents Chemother *56,* 1797-1809.

Typas, A., Banzhaf, M., van den Berg van Saparoea, Bart, Verheul, J., Biboy, J., Nichols, R.J., Zietek, M., Beilharz, K., Kannenberg, K., von Rechenberg, M.*, et al.* (2010). Regulation of Peptidoglycan Synthesis by Outer-Membrane Proteins. Cell *143,* 1097-1109.

Umare, M.D., Khedekar, P.B., and Chikhale, R.V. (2021). Mycobacterial Membrane Protein Large 3 (MmpL3) Inhibitors: A Promising Approach to Combat Tuberculosis. ChemMedChem *16,* 3136-3148.

van Kessel, J.C., and Hatfull, G.F. (2007). Recombineering in Mycobacterium tuberculosis. Nat. Methods *4,* 147-152.

Varadi, M., Anyango, S., Deshpande, M., Nair, S., Natassia, C., Yordanova, G., Yuan, D., Stroe, O., Wood, G., Laydon, A.*, et al.* (2022). AlphaFold Protein Structure Database: massively expanding the structural coverage of protein-sequence space with high-accuracy models. Nucleic Acids Research *50,* D439-D444.

Wu, K.J., Zhang, J., Baranowski, C., Leung, V., Rego, E.H., Morita, Y.S., Rubin, E.J., and Boutte, C.C. (2018). Characterization of Conserved and Novel Septal Factors in Mycobacterium smegmatis. J. Bacteriol. *200,* 10.1128/JB.00649-17. Print 2018 Mar 15.

Wuo, M.G., Dulberger, C.L., Brown, R.A., Sturm, A., Ultee, E., Bloom-Ackermann, Z., Choi, C., Garner, E.C., Briegel, A., Hung, D.T., Rubin, E.J., and Kiessling, L.L. (2022). Antibiotic action revealed by real-time imaging of the mycobacterial membrane.

Xu, Z., Meshcheryakov, V.A., Poce, G., and Chng, S.S. (2017). MmpL3 is the flippase for mycolic acids in mycobacteria. Proc. Natl. Acad. Sci. U. S. A. *114,* 7993-7998.

Zhang, Y.J., Ioerger, T.R., Huttenhower, C., Long, J.E., Sassetti, C.M., Sacchettini, J.C., and Rubin, E.J. (2012). Global assessment of genomic regions required for growth in Mycobacterium tuberculosis. PLoS Pathog. *8,* e1002946.

Zheng, S.Q., Palovcak, E., Armache, J., Verba, K.A., Cheng, Y., and Agard, D.A. (2017). MotionCor2: anisotropic correction of beam-induced motion for improved cryo-electron microscopy. Nat Methods *14,* 331-332.

Zuber, B., Chami, M., Houssin, C., Dubochet, J., Griffiths, G., and Daffe, M. (2008). Direct visualization of the outer membrane of mycobacteria and corynebacteria in their native state. J. Bacteriol. *190,* 5672-5680.

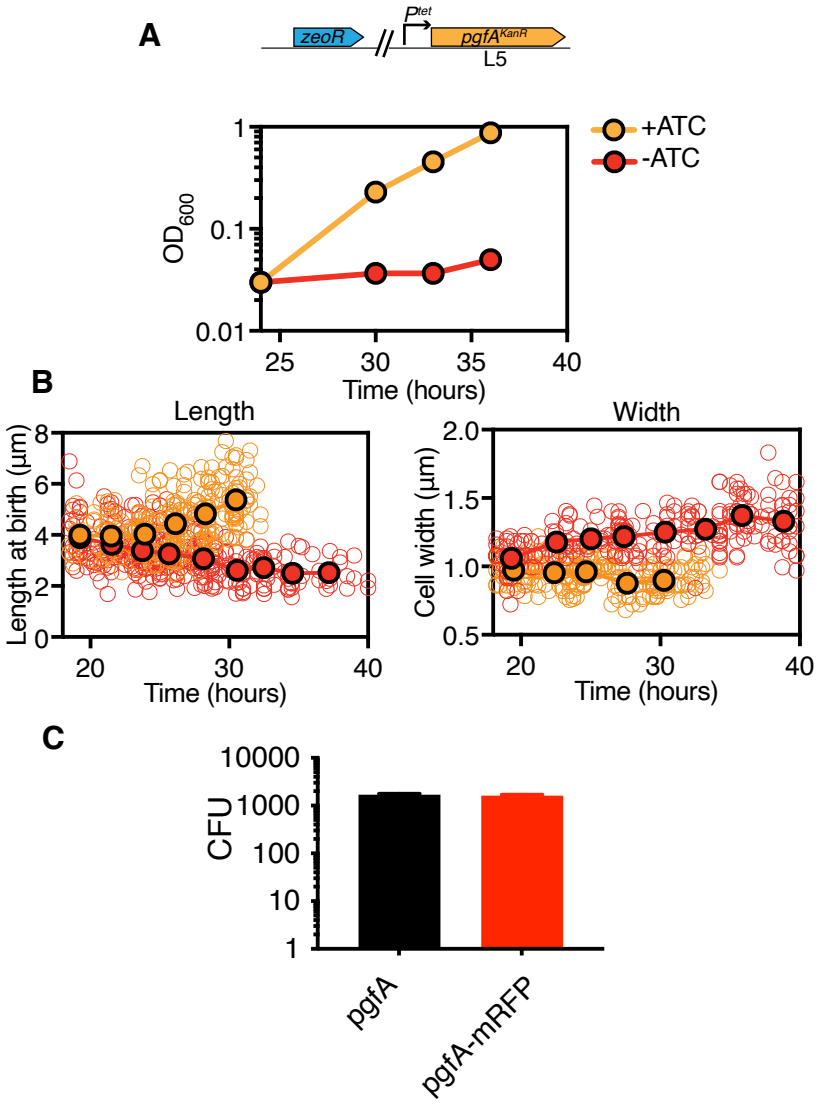


**Figure 1 – figure supplement 1. (A)** Optical density over time of a strain whose only copy of *pgfA* is tetracycline inducible, with and without ATC (+/-ATC). Points are means of three biological replicates. Error bars are too small to be visible. Experiment was performed at least 4 times on separate days, and representative data are shown. ATC=anhydrotetracycline. Time on the *x*-axis corresponds to time after ATC was removed. **(B)** Birth lengths and cell widths over time of depletion (orange = +ATC; red = -ATC). Open circles represent individual cells (length: N = 261 (length) & 253 (width) for +ATC; N = 355 (length) & 254 (width) -ATC). Closed circles are not fits to the data but represent the mean of cells in 2.25-hr (length) or 2.75-hr (width) bins. The experiment was performed twice on separate days. In +ATC cultures, cell density became too high to measure length and width past ~33 hrs. ATC=anhydrotetracycline **(C)** L5-allele swapping with *pgfA* or *pgfA-mRFP* expressed by the native promoter. Bars represent means of 3 biological replicates. Error bars indicate standard deviation.

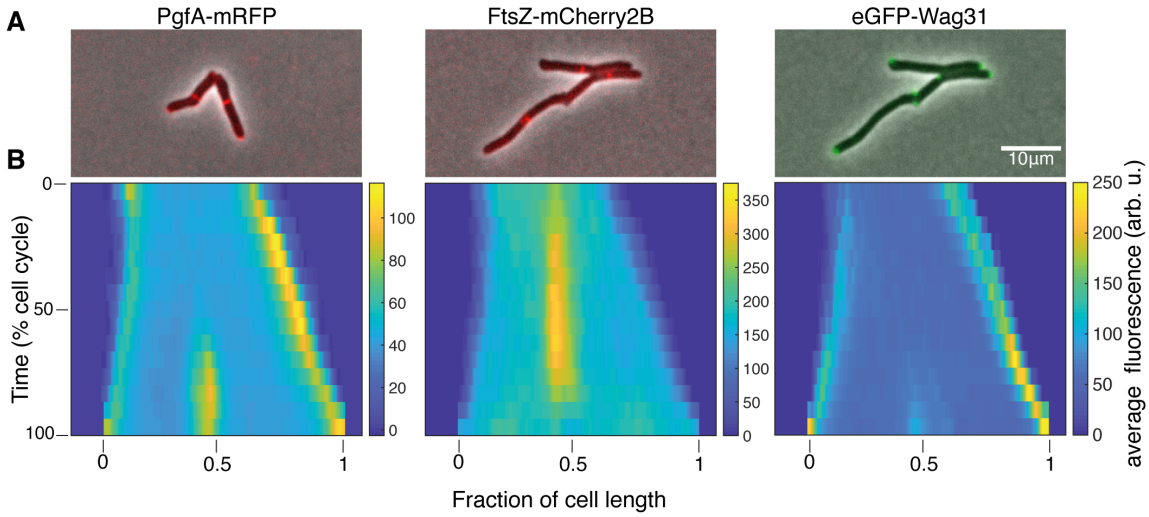


**Figure 1 – figure supplement 2** (A) Merged phase-contrast and fluorescence images of Msm cells expressing PgfA-mRFP, eGFP-Wag31 and FtsZ-mCherry2b. (B) Average fluorescent distributions over time (kymographs) from cells aligned from new to old poles and from birth to division (N=20 PgfA-mRFP; N=48 FtsZ-mCherry2B; N=20 eGFP-Wag31).

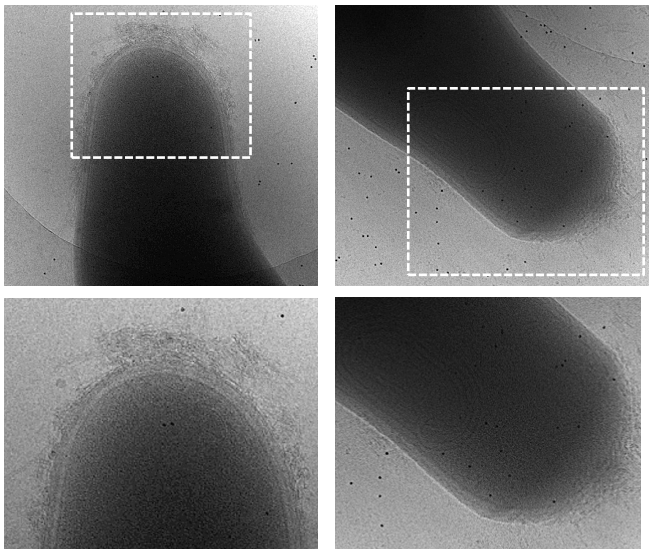

**Figure 2 – figure supplement 1.** The cell envelopes of PgfA-depleted show outer membrane wall fraying at 24 hours left) and 33 hours (right) of depletion.

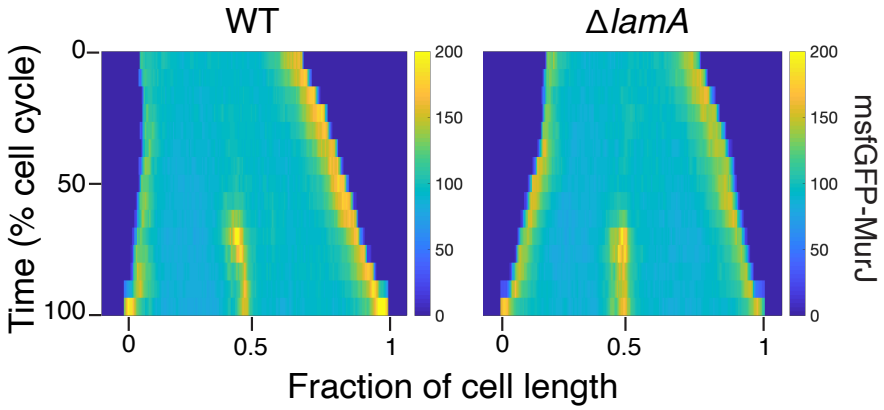


862
863
864 **Figure 2 – figure supplement 2.** Kymographs of a fluorescent fusion to MurJ in WT and
865 in Δ*lamA* cells. N=25.
866

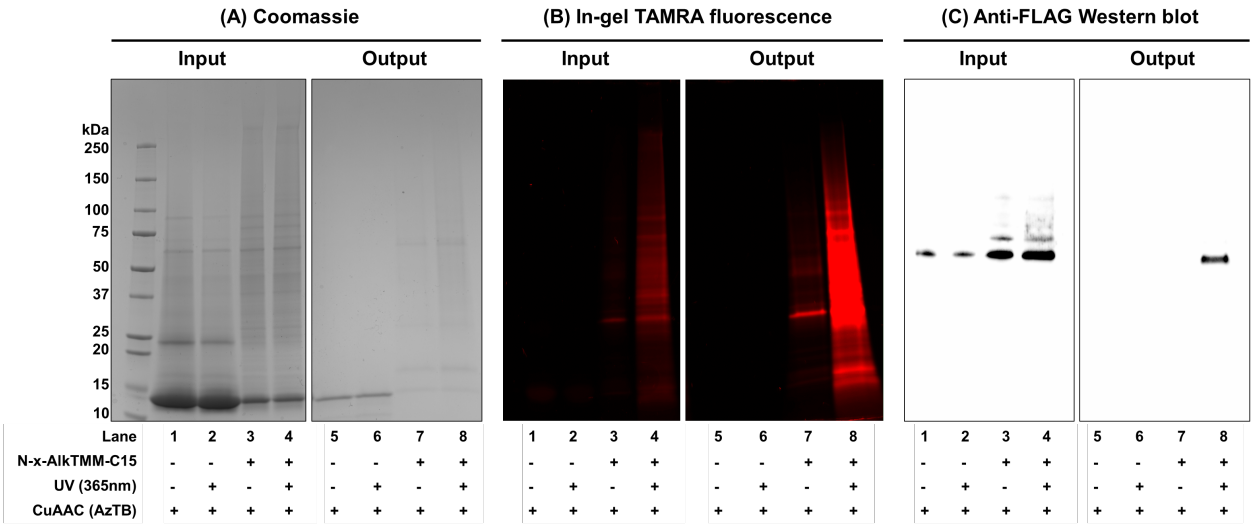


**Figure 3– figure supplement 1.** Full results of experiment present in Main text Figure 3A. Photoactivatable TMM analogue interacts with MSMEG_0317 in live *M. smegmatis*. KG167 expressing 3x FLAG-tagged MSMEG_0317 was cultured with N-x-AlkTMM-C15 (100 μM), UV-irradiated, and lysed. Lysates were reacted with azido-TAMRA-biotin reagent (AzTB) by Cu-catalyzed azide-alkyne cycloaddition (CuAAC “click” reaction), and analyzed before (input) and after (output) avidin bead enrichment. Input and output samples were analyzed by (A) Coomassie staining, (B) in-gel fluorescence scanning, and (C) anti-FLAG Western blot. Data are representative of two independent experiments. High-intensity band at low molecular weight in the Coomassie-stained gels represents lysozyme used in the cell lysis procedure.

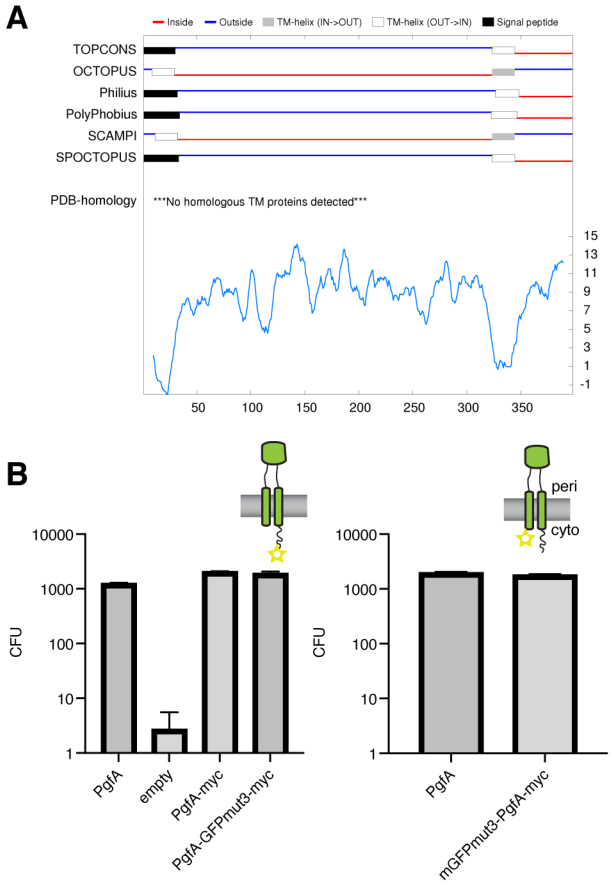


**Figure 3 – figure supplement 2. (A)** Output from TOPCONS (https://topcons.cbr.su.se/), which aggregates the results of several transmembrane prediction algorithms. The input is MSMEG_0317, or PgfA. **(B)** Results of allele swapping with the indicated PgfA fusion proteins.

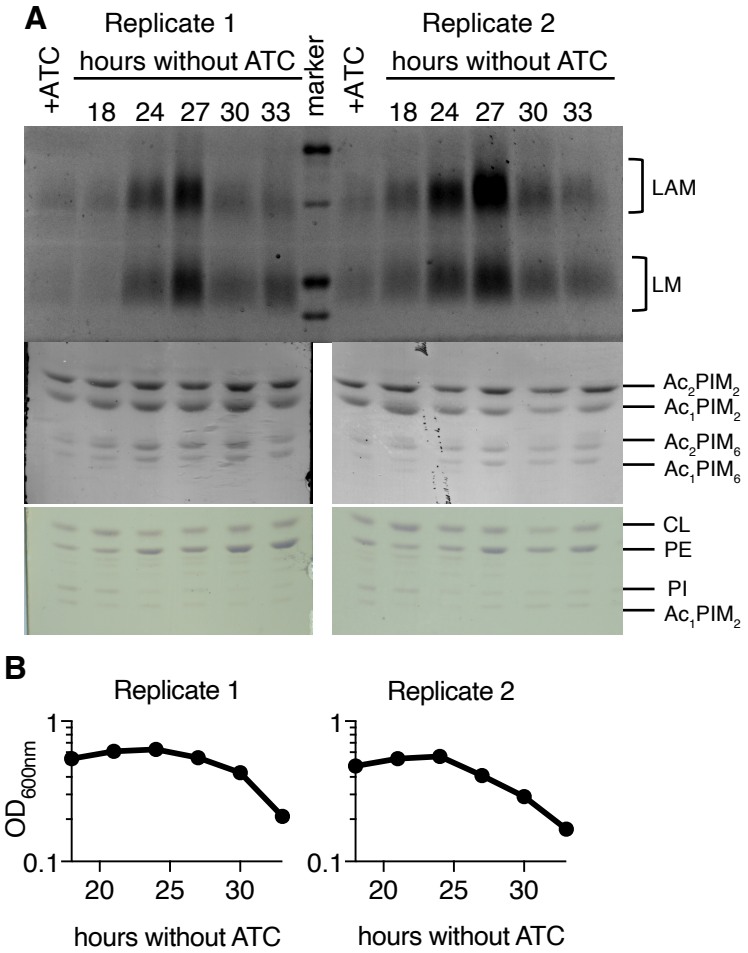


**Figure 4 – figure supplement 1.** Two additional biological replicates of LM/LAM analysis during PgfA depletion. **(A)** As in Main Text Figure 4A , LM/LAM and other lipids were extracted and separated by SDS-PAGE and TLC in cells expressing (+ATC) and depleted for (-ATC) PgfA. Two biological replicates are shown. (B) For the same replicates optical density was measured during depletion. To avoid changes in LM/LAM due to cell density, at the indicated timepoints, half of the cultures were taken for lipid analysis, and replaced with fresh media.

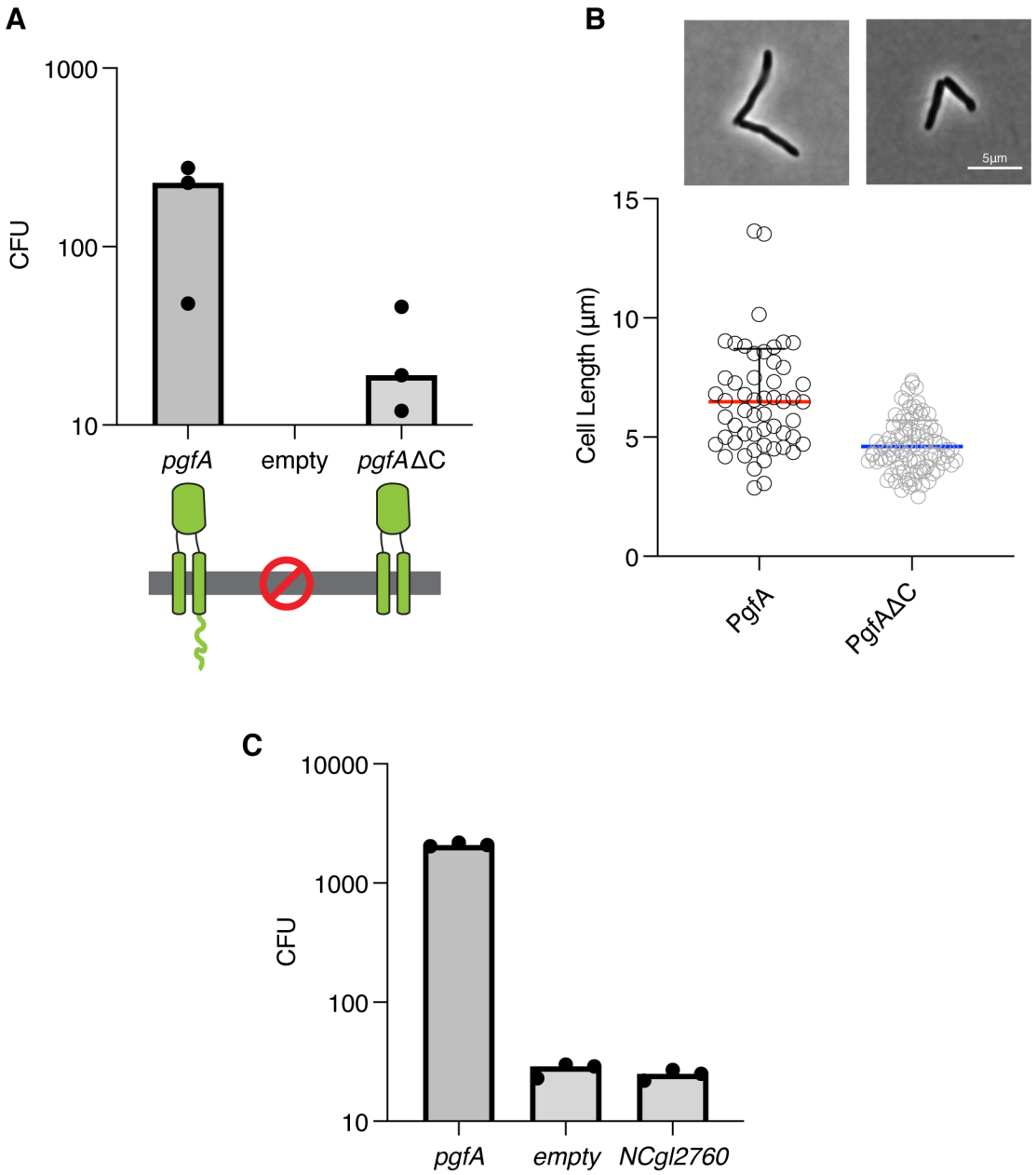


**Figure 4 – figure supplement 2. (A)** Results of exchanging the indicated *pgfA* alleles for a wildtype copy of *pgfA*. Bars represent medians. **(B)** Cell morphology analysis of a surviving transformant. Lines represent medians. **(C)** Results of exchanging the indicated *pgfA* alleles for a wildtype copy of *pgfA*. Bars represent medians.

**Figure 2 – video supplement 1:** Phase time-lapse microscopy of cells carrying ATC-inducible CRISRPi guides targeting either *pgfA* (left) or *mmpL3* (right). Exposure to ATC occurs at the beginning of the video.